HHS Public Access

Author manuscript

Brain Struct Funct. Author manuscript; available in PMC 2020 August 16.

Published in final edited form as:

Brain Struct Funct. 2018 July ; 223(6): 2949–2971. doi:10.1007/s00429-018-1671-8.

Connectivity of neuronal populations within and between areas of primate somatosensory cortex

E Pálfi[1], **L Zalányi**[2], **M Ashaber**[3,4], **C Palmer**[5], **O Kántor**[1,6], **AW Roe**[7,8], **RM Friedman**[7], **L Négyessy**[1,2]

[1]Department of Anatomy, Histology and Embryology, Semmelweis University, Budapest, H-1094 Hungary

[2]Complex Systems and Computational Neuroscience Group, Wigner Research Centre for Physics, Hungarian Academy of Sciences, Budapest, H-1121 Hungary

[3]Department of Physiology and Biochemistry, Szent István University, Faculty of Veterinary Science, Budapest, H-1078 Hungary

[4]Division of Biology and Biological Engineering, California Institute of Technology, Pasadena, CA, 91125, USA

[5]University of Montana, Department of Mathematical Sciences, Missoula, MT, 59812, USA

[6]Department of Neuroanatomy, Institute of Anatomy and Cell Biology, Faculty of Medicine, University of Freiburg, Freiburg, 79104, Germany

[7]Oregon Health and Science University, Division of Neuroscience, Portland, OR, 97006, USA

[8]Zhejiang University, Interdisciplinary Institute of Neuroscience and Technology, Hangzhou, 310029, China

Abstract

Functions of the cerebral cortex emerge via interactions of horizontally distributed neuronal populations within and across areas. However, the connectional underpinning of these interactions is not well understood. The present study explores the circuitry of column-size cortical domains within the hierarchically organized somatosensory cortical areas 3b and 1 using tract tracing and optical intrinsic signal imaging (OIS). The anatomical findings reveal that feedforward connections exhibit high topographic specificity, while intrinsic and feedback connections have a more widespread distribution. Both intrinsic and inter-areal connections are topographically oriented across the finger representations. Compared to area 3b, the low clustering of connections

Corresponding author: László Négyessy, Complex Systems and Computational Neuroscience Group, Wigner Research Centre for Physics, Hungarian Academy of Sciences, Adress: Konkoly-Thege Miklós út 29-33. 1121 Budapest, Hungary, negyessy.laszlo@wigner.mta.hu.

2)Disclosure of potential conflicts of interest: The authors declare that they have no conflict of interest.

3)Research involving Human Participants and/or Animals: This article does not contain any studies with human participants performed by any of the authors.

4)Ethical approval: All applicable international, national, and/or institutional guidelines for the care and use of animals were followed. Animal care and surgeries were performed according to NIH (National Institute of Health) regulations and were in compliance with and approved by the Institutional Animal Care and Use Committee of Vanderbilt University.

5)Informed consent: n.a.

and small cortical magnification factor supports that the circuitry of area 1 scaffolds a sparse functional representation that integrates peripheral information from a large area that is fed back to area 3b. Fast information exchange between areas is ensured by thick axons forming a topographically organized, reciprocal pathway. Moreover, the highest density of projecting neurons and groups of axon arborization patches corresponds well with the size and locations of the functional population response reported by OIS. The findings establish connectional motifs at the mesoscopic level that underpin the functional organization of the cerebral cortex.

Keywords

horizontal connections; cortical hierarchy; cortical magnification; optical intrinsic signal imaging; tract tracing

Introduction

In primary somatosensory cortex (SI) Brodmann areas 3b (BA3b) and 1 (BA1) are crucial for tactile perception (Sathian et al. 2016; Yau et al. 2016) and have been shown to be regions of important inter-digit interactions and submodality integration (e.g. Costanzo and Gardner 1980; Iwamura et al. 1983b, Chen et al. 2003; Sripati et al. 2006; Friedman et al. 2008; Reed et al. 2008; Pei et al. 2009; Lipton et al. 2010; Thakur et al. 2012;). In agreement with the physiological observations, tract tracing experiments indicate widespread connectivity in SI (Krubitzer and Kaas, 1990; Burton and Fabri, 1995; Manger et al., 1997; Fang et al., 2002). Recently we have shown that small injections of neuronal tracers restricted to a column size region of SI result in strong reciprocal connections not only within the injected distal finger pad representation, but also with neighboring distal finger pad regions in BA3b and BA1 (Négyessy et al. 2013; Ashaber et al. 2014). In contrast, between BA3b and BA1 high density reciprocal connections are restricted to the homotopic distal finger pad representations. Furthermore, using fMRI and electrophysiological approaches we have demonstrated that within these two areas there are two predominant streams of information flow, an intra-areal stream which integrates information from different digits and an inter-areal stream which integrates same digit information (Wang et al. 2013). Although, these findings show, that similar to the visual cortex in SI intrinsic connections have a larger lateral spread than inter-areal, it remains unclear whether the circuitry of SI is hierarchically organized and formed by feedforward and feedback connections exhibiting highly restricted and more extensive lateral spread, respectively (Angelucci and Bressloff 2006; Jeffs et al. 2009; Markov et al. 2014). The importance of lateral spread in connectional hierarchy and sensory cortical integration is shown by studies on the spatial organization of visual cortical receptive fields (Angelucci and Bressloff 2006). However, only a few studies in sensory cortex have examined the spatial relationship of hierarchically organized cortical connections (Cleland 2010; Hackett et al. 2014; Vincis and Fontanini 2016). One of the major goals of our studies is to better understand the convergence and divergence of intrinsic, feedforward and feedback connections in SI.

In this study we have further analyzed the anatomical connection patterns of column-size loci of the distal finger pad representations reported in our previous studies (Négyessy et al. 2013; Ashaber et al. 2014) to examine the distribution and clustering of projections relative to the somatotopic representations, and in this study, the cortical magnification factor (CMF, a measure of the size of a cortical area devoted to the processing of information from a unitary area of the sensory periphery), and therefore provide evidence that hierarchical sensory cortical processing is based on a canonical connectional motif. We use bidirectional tracing which provides an opportunity to study both the origin and termination of the connectivity within and between the areas. Also, by using a combination of complementary measures, especially given the small sample size which is characteristic of many primate studies, we specifically aim to shed light on 3 questions. (1) Is the widespread somatotopic and submodality integrations of SI reminiscent of the receptive field (RF) organization in visual cortex including most notably the extra-classical RF (ecRF)? In visual cortex feedforward connections form the RF center, while intrinsic and feedback connections are largely responsible for the surround organization including the ecRF (for a review see Angelucci and Bressloff, 2006). The assessment of the lateral spread of the projections between two interconnected areas as made in the present study allows for this comparisons in projection patterns, which are not possible with an injection of a single area. (2) Is there a clustering of connections that reflect the functional selectivity in SI that is akin to that shown for the submodality specific, columnar-like distribution of connections within and between primary visual cortical areas (again, for a review see Angelucci and Bressloff 2006)? It is known that the distribution of intrinsic connections is anisotropic and oriented along the orientation axis in the retinotopic map of V1 (Sinchich and Blasdel, 2001) and across the distal finger pad representations in SI (Négyessy et al. 2013; Wang et al. 2013; Ashaber et al. 2014). However, it is less clear whether the distribution of the inter-areal connections exhibits similar functional specificity. (3) Is the circuit basis of the cortical population response in SI similar to the basis of the visual population receptive fields (pRF) highlighted by recent high resolution fMRI findings in the visual cortex suggesting that interactions between cortical areas depend on a unit size of cortical tissue representing a population response (Harvey and Dumoulin 2011; Wandell and Winawer 2015)? For this, we compared the lateral spread of the intra-areal, feedforward and feedback connections to the size of the cortical response recorded by intrinsic signal optical imaging (OIS, Chen et al. 2003; Friedman et al. 2008; Rasch et al. 2013). Further establishing the fMRI findings will be especially important in understanding the circuitry underlying high resolution fMRI observations. Parts of these results have been published in abstract form (Négyessy et al. 2015, 2016; Pálfi et al. 2016).

Materials and methods

Experimental procedures

Three female (J, V, M) and three male (Mc, P, Mo) adult squirrel monkeys *Samiri sciureus* were used in this study. Animal care and surgeries were performed according to NIH (National Institute of Health) regulations and were in compliance with and approved by the Institutional Animal Care and Use Committee of Vanderbilt University. The intrinsic optical imaging and electrophysiological methods used to map the somatotopy of the somatosensory

cortical areas have been described previously (Négyessy et al. 2013; Ashaber et al. 2014). Borders between cortical areas were estimated based on electrophysiological mapping, receptive field characteristics, and optical imaging as described previously (see Fig. 1 in Négyessy et al. 2013). Considering the known somototopic organization of SI (Sur et al., 1982; Merzenich et al., 1987; Chen et al., 2001), the border between BA3b and BA1 were drawn across the representation of the base of the fingers and the palm. All monkeys received an iontophoretic injection of biotinylated dextran amine (BDA, 1:1 mixture of 10K and 3K) into a cortical distal finger pad representation, among which three cases were injected into BA3b (J, Mc, V) and the other three into BA1 (M, Mo, P). The locations of the BDA injections were guided by functional maps obtained using OIS and electrophysiological receptive field recordings (Fig. 2). Injections were delivered into a cortical site exhibiting SAI response properties. Histological procedures were made on series (roughly 10 sections per case) of regularly spaced (130–160 μm except one case with 270 μm), 50 μm thick sections cut in the tangential plane (parallel with the cortical layers). BDA was revealed by the avidin-biotin peroxidase (ABC) protocol using Ni intensified diaminobenzidine (DAB) as the chromogen. Then sections were osmicated, dehydrated and flat embedded in resin. Anterograde and retrograde labeling were mapped with Neurolucida® (MicroBrightField Europe, E.K. Magdeburg, Germany). The anatomical and functional maps were aligned and the connectivity analyzed on the combined maps. Alignments were made in Neurolucida and Adobe Photoshop (Adobe Systems Incorporated, San Jose, CA). Only BA3b and BA1 were studied. After mapping the anterograde and retrograde labeling, blocks including the BDA labeled axonal processes were dissected from the sections and cut with an ultramicrotome for transmission electron microscopic (EM) examination after staining the ultrathin sections with lead-citrate. For more details including the sources of reagents see Négyessy et al. (2013) and Ashaber et al. (2014).

Alignments

Panoramic microscopic images of the sections, taken at 4x objective magnification, were used to decrease the distortion resulting by spherical aberration. Sections were aligned to each other using the injections site, visible electrode penetrations and the pattern of cross or tangential sections of blood vessels. The pattern of horizontally running blood vessels on superficial sections were matched with the blood vessels on an image of the brain surface centered on the injected region. This step was performed in Photoshop, which allowed for rescaling of the images to equal their size. Mappings of labelled structures were made using the serial section reconstruction function of Neurolucida. This function allows alignment of consecutive sections with high precision. Finally drawings of the Neurolucida reconstructions were scaled and aligned with images of the serial sections and thereby with the image of the brain surface. This procedure resulted with high precision an alignment of the images centered around the injection site including neighboring area 3b or 1, which was the focus of this study. However, precision became less reliable in regions distant from the injection site due mainly to the peripheral distortion of the image taken of the cortical surface; these regions fell outside of the area used for the analyses of the labeling. More detailed description of the alignment is provided in Négyessy et al. (2013).

Data analyses

Within the region of interest all BDA labeled neuronal elements including retrogradely labeled cell bodies, axonal fibers (anterograde labeling) and patches of terminal axon arborizations (axonal patches), which were mapped and reconstructed with Neurolucida, were considered in the analyses. Analyses were made either by ignoring the laminar positions (merging the full series of sections) or separately for the supra- and infragranular cortical layers by merging the corresponding sections of the series (described in detail below).

The quantitative analysis of the retrograde labeling focused on labeled neuronal somata within regions of high labeling density, which were defined by using a graded kernel density analyses as described below in subsection “Analysis of the spread of retrograde labeling” and shown in Figure 1. BDA labeled neurons localized in regions of low labeling density were excluded from the analyses. The excluded regions only contained 1.3% of the labeled neurons on average, representing territories with very low connectional probabilities. Also, labeling within the core of the injection site, that measured 300 μm in diameter, was omitted from the analyses to avoid the consideration of structures labeled directly by the BDA injection and not by neuronal transport.

Measuring the densities of bouton-like structures within axonal patches have been described previously (Négyessy et al. 2013; Ashaber et al. 2014). In short, boutons were counted in 3 neighboring, 50 μm^2 sampling rectangles (i.e. 150 μm^2) using a 100x objective in the full depth of the sections. As sampling was focused on the neuropil, the rectangles were placed in a way to avoid the inclusion of blood vessels and labeled perikarya. Similarly, labeled dendritic processes, which could fully or partly occlude the field of view, were also avoided during the placement of the rectangles.

Calculation of the fraction of labeled structures in the cortical layers and areas—The criteria for classifying horizontal sections as supragranular or infragranular was the appearance of large BDA labeled pyramidal cells characteristic of layer 5. Sections above the one including large BDA labeled pyramidal cells were considered supragranular with the rest as infragranular. The granular middle layer was not possible to determine in every series of sections as it may have been lost due to the sampling. Therefore in some of our series middle layers could have been included with the supragranular sections and not in others lacking sections through granular layer 4. Following the logic of Barone et al. (2000) the ratios of the supragranular labeling of neurons, axonal patches and bouton-like structures were determined relative to the total number of each structure counted across the full series of sections (i.e. counts in supragranaular plus infragranular sections) separately in BA3b and BA1. The areal distribution of the labeled structures was calculated as the proportion of the total number counted in the two areas (BA3b and BA1) together.

Within BA3b and BA1 the fraction of projection neurons labeled within the sensory elicited OIS-area, a measure of the population receptive field, was calculated. In case V OIS experiments did not produce a measurable signal in BA1. Therefore, for this case the size and location in BA1 of a sensory activated OIS-area was estimated by drawing a circle

around the center of mass of the highest density retrograde labeling (defined and described below) with a size of an average BA1 OIS-area (Friedman et al. 2008).

Analysis of the spread of retrograde labeling—The Voronoi tessellation used in our original analyses (Négyessy et al. 2013; Ashaber et al. 2014) produced a patchy pattern of the highest density regions, which cannot be unequivocally delineated for determining the size of an area. In order to measure the spread of retrograde labeling we applied kernel smoothing based on a Gaussian distribution. As shown in Figure 1 Gaussian smoothing is a reasonable choice as the density of the distribution of labeled neuronal structures is apparently Gaussian-like around the injections site (see also Barone et al. 2000; Buzás et al. 2006; Horvát et al. 2016). Similarly, retrograde labeling of the long range inter-areal connections also exhibits a Gaussian-like distribution (Barone et al. 2000). Kernel density analysis allowed a delineation of the area with the highest density retrograde labeling both within the injected and interconnected area studied (Fig. 1). Kernel density maps were computed as follows. First, a convolution with the Gaussian kernel (σ = 280 μm) was applied over the registered neuron positions to generate a surface "density" map. The parameter σ was chosen to acquire the best correspondence between the kernel density map and the Voronoi based density maps in our previous studies (Négyessy et al. 2013; Ashaber et al. 2014). The size 1800x1800 μm^2 was adjusted then to include the region of interest with valuable kernel density measures. Next we normalized the *values* of the resulted surface heights yielding a maximum value 1 to ensure the comparability among measurements from the different monkeys.

$$D_{map}(x,y) = \int G(x',y',\sigma) \sum \delta\left(x_{neuron_j} - x - x', y_{neuron_j} - y - y'\right) dx'dy'$$

$$\widehat{D_{map}} = D_{map}(x,y) / \left(\max_{x,y} D_{map}(x,y)\right)$$

D_{map}: density map, G(x,y,σ): Gaussian distribution with μ: (x,y) and σ; d(x,y): Dirac delta function. $\widehat{D_{map}}$: normalized D_{map} function. The normalized "density" map is a relative map, it shows the spatial density relative to the maximal density of the projection neurons. As the normalized density values showed a wide range of values (only a few small areas had high density i.e. near 1; whereas others exhibited very low density values) a logarithm of the density values was used to aid visualization. On the figures (Figs. 1, 2) the color code represents the values of the log densities ranging from the highest density [−0.5 to 0] to the lowest density [−6.5 to −7.5]. Eight different densities ranging from 0 to −7.5, were defined (Fig. 1) from which only the highest 4 were used in the present analysis; the log value of the lowest [−3.5 to −2.5] density range was 0.78 to 3.1% of the highest density value (Fig. 2).

For each case density maps were computed by merging the full series of horizontal sections, thereby ignoring cortical depth. To measure the size of the spread of retrograde labeling on the kernel maps the average Feret diameter and area values were calculated either with MATLAB (Mathworks, Natick, MA) or ImageJ (NIH, Bethesda, MD) .

Analysis of the spatial grouping of the retrograde labeling—Density-based spatial clustering (DBSCAN, https://en.wikipedia.org/wiki/DBSCAN, Ester et al. 1996) was used to study the compartmentalization of the retrogradely labeled neurons in BA3b and BA1. DBSCAN groups points, in our case retrogradely labeled neurons, that are closely packed. Instead of identifying clusters per se, we used DBSCAN to compare the clustering propensity of the projection neurons. An advantage of DBSCAN is that it does not require any presumptions about the number of clusters, and that it is not sensitive to the size, shape or localization of clusters, which makes it preferable to other binning based or k-means clustering techniques. Specifically, cluster size distribution and variability were compared. DBSCAN requires the specification of a length scale parameter, which determines the maximal distance between a point and at least a certain number (in our case 3) of closest neighbors. The shortest length scale was set to 4 μm that was incrementally changed by 8 μm to 700 μm. A cluster is formed by grouping points where all points have a close neighborhood set by the length scale and all points are reachable from any other point within the cluster (Fig. 3). In our study, clustering was studied as the function of the length scale, instead of selecting a single specific value, avoiding one of the major disadvantages of DBSCAN. We investigated cluster density variability with two methods: 1) by counting the number of clusters disregarding their sizes and 2) by characterizing the cluster size distribution. Size was defined by the number of neurons within a cluster. To evaluate the variability of the cluster size distribution at each length scale its entropy was computed based on the probability that a randomly selected cluster would have a certain size. The number of clusters of a given size is described with N_s, so the probability that a randomly selected cluster has a size equal to s is $p(s) = N_s / \sum_k N_k$. The entropy was then calculated from this probability distribution as follows: $H = -\sum(p_s * log_2(p_s))$. The median of the distributions measured from the different injections (i.e. three cases per injection of the two areas) were plotted separately for the intra-areal and inter-areal labeling.

Analysis of the spread of anterograde labeling—The spread of anterograde labeling was evaluated with the distribution of the axonal patches, which have the highest density of bouton like structures compared to other regions outside of the patches (Négyessy et al. 2013; Ashaber et al. 2014) and form the specific target regions of an injected cortical site. Similarly as in case of the retrograde labeling, analysis of the anterograde labeling was performed separately in the two somatosensory areas after the two different injections. To select the highest labeling densities, i.e. the most effective target sites, only groups formed by overlapping axonal patches appearing in the same horizontal localization in more than one section of a series (i.e. in different depths) were considered (Fig. 2); thus, single patches were omitted from the analyses (except in anisotropy measures, see below). For these measurements first we defined the center of mass of the axonal patch groups in all cases with MATLAB. To define the spread of anterograde labeling we computed: 1) the average neighborhood distance of the center of mass of the patch groups by the nearest neighbor function in Neurolucida Explorer (computes distance only for the closest neighbor) (Fig. 8a) and 2) the average distance of the center of mass of the patch groups from the injection site in case of the intra-areal labeling or from the center of mass of the highest density retrograde labeling on the kernel maps in case of the inter-areal labeling (Fig. 8b). Notably, in the case of inter-areal labeling the center of mass of the highest kernel density region was located

within the homologous cortical representation of the injected finger pad representation (Négyessy et al. 2013; Wang et al. 2013; Ashaber et al. 2014). The relationship between the spatial distribution of groups of axonal patches and retrograde labeling density was investigated, after map alignment, by counting the number of patch groups that fell within full range of kernel density regions (i.e. not only the 4 highest). When a patch group overlapped two kernel densities half values were assigned to each density. To gain a better insight into this relationship of the intra-areal and inter-areal labeling, kernel densities were ranked in each area beginning with the highest value of labeling where there occurred overlap with a patch group.

Measuring anisotropy—Anisotropy was computed according to Sincich and Blasdel (Sincich and Blasdel 2001) separately for the intra-areal and inter-areal labeling. This normalized measure is the vector average of the radii between a center point and the pointwise representation of labeled structures, i.e. axonal patches and projection neurons. Patch anisotropy was computed by using the center of mass of each patch separately for all the patches including both the single ones and those forming axonal patch groups. For the intra-areal labeling, anisotropy of the neuronal and axonal patch distributions were computed relative to the injection site, while for the inter-areal labeling the center of mass of the highest density of retrograde labeling was used as the center point (Fig. 10a, d). The length of the vector defines the ellipticity of the distribution while its angle shows the major direction of the orientation of the connectional spread. It provides a value of 0 if the labeled structures are located symmetrically around the center and yields 1 if all the centers are arranged along a straight line. The angle of the anisotropy vector was measured relative to the border between BA3b and BA1, which is roughly orthogonal to the representation of the individual fingers.

Mapping thick axonal processes

BDA labeled, horizontally running thick axonal fibers were mapped by Neurolucida and then polar plots of their distribution were generated with Neurolucida Explorer. The polar plots of the different cases with injections into the same area were then centered around the injection sites and superimposed using different landmarks similarly as in the alignment procedure described in our previous studies (Négyessy et al. 2013; Ashaber et al. 2014). This method allowed for the calculation of the orientation of the labeled, overlapping axons. After mapping was completed, selected regions of the different cases were cut for electron microscopy and several examples of the labeled axons were examined for the presence of a myelin sheath.

If not mentioned measurements and analyses including statistical comparisons were made by Neurolucida Explorer, ImageJ and/or MATLAB and MS Excel. If not noted otherwise statistical comparisons were made by two way of ANOVA and t-test.

Results

1. Qualitative observations

Figure 1 shows the distribution of retrograde (small black triangles in a and c) and anterograde (gray shading in B and D) labeling in 2 cases, one with a BA3b (a–b) and the other with a BA1 (c–d) injection after aligning and collapsing the serial tangential sections. The labeled structures are shown superimposed on the kernel density maps of the retrogradely labeled neurons. The kernel density analysis confirmed that the highest density of BDA labeled neurons was centered around the injection site and the high density inter-areal labeling was located at the homologous finger pad representation. After BA3b injection the majority of neurons projecting to this site were intra-areal and centered around the injection site with the addition of more distal intra-areal neurons as well as inter-areal neurons originating in BA1 (Fig. 1a). The distribution of intra-areal neurons labeled after BA1 injection was more broadly distributed and in contrast to the BA3b injection there was a large contingent of inter-areal projecting neurons (Fig. 1c). Reconstruction of the anterograde labeling revealed that for both cases injections in BA3b and BA1 led to a broad intra-areal distribution and either a more focused or broader inter-areal distribution of the axonal patches (Fig. 1b, d).

To evaluate the reciprocal connections between BA3b and BA1 we were interested in comparing regions with the highest density of projection neurons and axonal patches. Selecting only the 4 highest density regions for analysis excluded low density regions that had retrograde labeling density values that were less than 1% of the peak (for corresponding neuronal numbers see the Methods section). Identification of well-defined axonal patches was used to locate regions with a high density of bouton-like structures (Négyessy et al. 2013; Ashaber et al. 2014). Figure 2 shows for the 3 cases with BA3b injection (a) and the 3 cases with BA1 injection (b) the color coded kernel density maps of the highest retrograde labeling densities of projection neurons along with the distribution of the anterogradely labeled groups of axonal patches (thin outlines) used in our analyses. For all cases the injection sites (white star) were localized within the targeted cortical area activated by tactile stimulation as revealed in OIS experiments (OIS-area, thick outline) with one exception, case P, where the BDA-injection was localized within the distal finger pad representation as determined by the electrophysiological mapping (Ashaber et al. 2014) (Fig. 2). In line with our previous observations (Négyessy et al. 2013; Ashaber et al. 2014) Figure 2 suggests the following qualitative observations: (1) the large red areas around the injection sites indicate that the density of intra-areal neuronal projections in BA3b or BA1 was greater than inter-areal (note the lack of the red areas or its small extent in the single case M in the non-injected area), (2) the density of neuronal labeling was especially high in BA3b when comparing the intra-areal and the inter-areal labeling after BA3b and BA1 injections, (3) the co-localization of the high kernel density and the OIS-areas (white and black contours) shows that inter-areal neuronal projections were originating largely from the homotopic cortical representation of the finger pad, (4) inter-areal axonal patches (light grey outlines) targeted the homotopic cortical representation in BA1 and exhibited larger spread including regions outside the OIS-area in BA3b and (5) intra-areal axonal patches also showed a widespread lateral distribution. However, please note that regarding points 4 and 5, only

groups of overlapping axonal patches are shown (see Methods and section 2 of the Results) and in some cases (intrinsic connections of case P and inter-areal patches of cases M and Mo) the inclusion of the single patches clearly shows the described patterns (Ashaber et al. 2014). These qualitative observations provided the basis of our quantitative analyses.

Seven measurements were made to compare the spatial characteristics of the distribution of the retrogradely labeled projection neurons and the anterogradely labeled axonal patches of the efferents of an injected locus: 1) areal and laminar proportional distributions of labeled structures, 2) clustering properties of projection neurons and efferent axonal patches, 3) lateral spread of projection neurons, 4) lateral spread of efferent axonal patches, 5) direct comparison of the spread of projection neurons and axonal patches, 6) direct comparison of the spread of projection neurons and axonal patches to the OIS-area and 7) anisotropic distribution of the projection neurons and efferent patches within and between the cortical areas. The lateral spread of connections were compared both in terms of cortical size as well as functional space by calculating the represented skin size with the aid of CMF values.

2. Areal and laminar distribution of the BDA labeled structures

We first quantitatively evaluated the distribution of the BDA labeled structures between cortical areas and layers to confirm the visual observations (Figure 2) and determine whether the proportional distribution of projection neurons and efferents could provide information about the relative strength of the connectivity and hierarchy (Markov et al. 2011; 2013) between BA3b and BA1. The findings are summarized in Figure 4.

The majority of projection neurons (ratio of neurons) were localized within the injected cortical area (one-tailed t-test, $p << 0.01$, Figure 4a), which is in agreement with previous observations (Markov et al. 2011; 2014). Furthermore, as shown in Figure 2 in the individual cases for both BA3b and BA1, the density of intra-areal neurons projecting to an injection site (BA3b or BA1) was greater than the inter-areal projections. Interestingly, relative to intra-areal connections, inter-areal labeling density was relatively higher with a BA1 injection as compared to that with a BA3b injection; there was a 1–3 order of magnitude difference between intra-areal and inter-areal labeling densities following BA3b injections, compared to 0–2 for BA1 injections (counts of the color coded log scale differences between the intra and the inter-areal densities in the different cases on Fig. 2).

Laminar analysis showed that most intra- and inter-areal neurons projecting to a BA3b or BA1 injection site originated in supragranular layers, Fig. 4b). There was no significant difference in the laminar distribution between the intra-areal projection neurons of BA3b and BA1 and the inter-areal projection neurons after BA3b and BA1 injections. The prevalence of supragranular labeling of neurons is in accordance with the literature (Burton and Fabry 1995). The minor differences between areas supports the hierarchical distance rule of Barone et al. (2000) (the closer of the hierarchical rank of two areas the more similar of the supragranular layer ratio). However, in contrast to expectations (Barone et al. 2000; Vezoli et al., 2004) BA3b injections resulted in significantly higher supragranular labeling of feedback neurons in BA1 compared to intra-areal labeling (one-tailed t-test, $p = 0.01$). In contrast, feedforward projection neurons within BA3b exhibit a similar supragranular ratio to the intrinsically projecting neurons after BA1 injection. Note, however, that these data were

obtained from an incomplete, regularly spaced series of sections cut parallel with the cortical layers.

Compared to neurons projecting to an injection site (Fig. 4a), projections from an injection site, as revealed by BDA-labeled axonal patches, showed that intra- and inter-areal efferent connections were more evenly distributed (ratio of patches, Fig. 4c). Overall, there was a tendency of labeling a greater proportion of efferent axonal patches in BA3b than BA1. A BA3b injection resulted in a greater number of intra-areal axonal patches than feedforward BA1 patches. In contrast, BA1 injection lead to a slightly greater number of feedback BA3b axonal patches than intrinsic BA1 patches. Akin to the retrograde labeling of neurons (Fig. 4b), efferent patches were found preferentially in supragranular layers (Fig. 4d). BA3b showed a greater tendency to send efferent axonal patches to supragranular layers than BA1 without either showing intra- or inter-areal differences. Further analysis, by taking into consideration the density of bouton-like structures within patches, found that the number of intra- and inter-areal axonal boutons were split relatively evenly (Fig. 4e) with only a slightly greater number of intra-areal than inter-areal boutons. Boutons were preferentially located in supragranular layers (Fig. 4f). With BA1 injections there appeared to be a wider spread of boutons into the infragranular layers for inter-areal feedback projections than intrinsic projections. The laminar distribution of the BDA-labeled axonal patches supported the hierarchical rank of two areas (Felleman and Van Essen, 1991). Although, the areal distribution of axonal patches also suggested a hierarchical organization, this observation has to be confirmed on more complete and larger data set.

3. Clustering of efferents and projection neurons

Clustering of the axonal patches—Examination of the merged series of sections showed that axonal patches exhibit a strong tendency to form groups of overlapping patches (Fig. 2). For most cases single patches accounted for only 15% to 17% of the total number of axonal patches as shown in Figure 5a. There was a trend for a lower frequency of overlapping patches intra-areally after BA1 injection. However, there were no statistical differences in overlapping patch frequencies irrespective of whether the injection was in BA3b or BA1 or whether the patches were intra- or inter-areal (feedforward or feedback). Interestingly, a closer look at the overlap revealed that efferent patches were found at the same spatial localization on the consecutive sections of a series, which suggests a columnar-like distribution pattern for both intrinsic projections as well as feedback and feedforward inter-areal projections.

We also observed that the groups of overlapping axonal patches varied in size, as defined by the number of overlapping patches on the series of sections (Fig. 2). To evaluate whether after BA3b or BA1 injection intra-areal and inter-areal labeling consisted of axonal patch groups of different sizes, cumulative frequency plots were generated to show the relative contribution of the different sizes of patch groups to the total number (Fig. 5b). Notable differences in the cumulative frequency distributions were found between the intra- and inter-areal labeling. Intra-areal labeling of the efferents mostly consisted of small groups of 2–3 patches. Patch group size 2 and 3 contributed about 50%−60% of intra-areal labeling compared to 20% of the total number for the inter-areal labeling. In contrast inter-areal

labeling was characterized by larger groups consisting of 5 or more patches. For inter-areal axonal patches the 60% total was reached at group size 5 and 7 following injection of BA1 and BA3b, respectively, where 40% of the total consisted of patch sizes of 8 and above. Note that the difference between the intra-areal and inter-areal distribution of the patch group size was larger after BA3b injection than after BA1 injection (Fig. 5b). With these differences in patch size, feedforward axonal patches apparently were distributed more homogenously across cortical layers than feedback and intrinsic efferent axonal patches.

Clustered distribution of the projection neurons—To address the question of spatial grouping of projection neurons we applied a density based clustering algorithm DBSCAN which groups together points (i.e. retrogradely labeled neurons) that are closely packed (Fig. 3). By varying a length scale parameter (from 4 μm to 700 μm by steps of 8 μm), which specifies the maximal distance between a point and its closest neighbors, we were able to systematically evaluate without assuming a cluster size the potential: (1) number of clusters, (2) cluster size distribution, and (3) entropy of the size variability of the resultant clusters. Figure 3c and d show that as a function of the length scale parameter the neuronal cluster number reached a peak very quickly and then at larger length scales the number dropped steeply (Fig. 3c, d insets) to a few number, which indicates the appearance of a large central cluster flanked by some smaller ones (as visualized in Fig. 3a, b), before converging towards 1. There are three observations of note: (1) Peak and total number of intra- and inter-areal spatial neuronal clusters were greater within BA3b than in BA1 irrespective of the injected area; (2) Total number of intra-areal neuronal clusters were greater than the number of inter-areal clusters; (3) Cluster number of intrinsically projecting neurons of B3b showed a faster decay with the length scale when compared to all the other conditions (Fig. 3c,d and insets). However, note that the measure of cluster number can be heavily influenced by the number and packing density of labeled neurons which was relatively large in BA3b (Fig. 2). Importantly, the density differences could have resulted in the cluster number peaking at different length scales. With BA1 having a lower labeling density, this could have contributed to the peak for intra-areal (inset of Fig. 3c) and inter-areal (Fig. 3d) labeling at larger length scales in BA1 than in BA3b. Also note that the large decay rate of the cluster number with the length scale for the intra-areal labeling suggests a quick formation of a large central cluster in BA3b relative to that seen in BA1 (insets in Fig3c, d), which is in agreement with the exponential decay rate of intrinsic labeling density as a function of distance from the injection site (Figs. 1,2; Horvát et al. 2016). For the inter-areal clustering the slight difference in the slopes (insets in Fig3c, d) may be due to a difference in the peak values and the lower labeling density in BA1 than in BA3b.

We quantitatively measured the variability of cluster sizes to determine whether the spatial distribution of the projection neurons were related to some regularity of the underlying cortical structure as e.g. a columnar representation or were founded in common connectional featural networks that would lead to a large diversity in cluster sizes. To estimate the size variability of the neuronal clusters, entropy was measured for each length scale. Entropy quantifies the uncertainty, i.e. the diversity present in the cluster size distribution independent of the actual probability distribution. Even with the large difference in the number of spatial clusters of neurons observed after BA3b and BA1 injections (Fig. 3c, d),

entropy of the cluster size distributions were quite similar for both (Fig. 3e, f), especially for the smaller spatial length scales (up to about 200 μm, Fig. 3e, f). The similar cluster size diversity again could be explained by the exponential distance rule (Horvát et al. 2016) resulting in the gradual emergence of a large central cluster via the fusion of numerous small ones. The entropy associated with the intra-areal cluster of neurons (Fig. 3e) was slightly greater than the inter-areal entropy (Fig. 3f). The diversity of the cluster size distribution was also highest around the length scale showing the peak number of clusters; however, in contrast to the number of clusters that falls off sharply with the length scale (Fig. 3c, d), the diversity showed only gradual decreases for both intra-areal (Fig. 3e) and inter-areal labeling (Fig. 3f). Consequently, a relatively large diversity of cluster size appears at larger length scales where the cluster number is relatively low, even when ignoring length scales above about 200 μm, where due to the low number of clusters entropy estimates become inaccurate. After the peak the slow decrease of the entropy compared to the steep decline of the cluster number indicates the formation of a large central cluster and a slowly decreasing number of small satellite clusters, which gradually melted into one central cluster as the function of the length scale increased (above about 500–600 μm) (Fig. 3c, d).

4. Lateral spread of the projection neurons

Size of the spread of neurons projecting to a cortical locus—To examine the spatial summation of neuronal projections to an injection site, the spread of the high density labeling (e.g. the areas enclosed by the dotted contours in case of J in Fig. 6a) was measured with the kernel density maps. In the comparisons of the feedforward and feedback connections within and between BA1 and BA3b, the most obvious observation was that the spread of intra-areal projections was larger than inter-areal (Fig. 6c, two way, repeated measure ANOVA, $p = 0.05$). Post hoc comparisons revealed the statistical difference between the intra-areal and inter-areal values only after BA3b injections (one-tailed t-test, $p = 0.008$). Affecting our measures was a single BAI injection case that exhibited an extremely large kernel area size for the intrinsic connections (Fig. 6c). More cases are needed to clarify this discrepancy. The size of cortical area providing inter-areal feedback connections from BA1 also tended to be greater than feedforward connections from BA3b to BA1.

To more directly relate the physical size of the cortical spatial summation to center-surround interactions properties of the receptive fields in BA3b and BA1, cortical magnification factors CMFs (mm cortex/mm skin) were used to calculate the cortical representation of the skin surface area providing connections to an injection site. Taking into account cortical magnification factors (CMFs (mm cortex/mm skin): 0.16 in BA3b and 0.06 in BA1, Friedman et al., 2008) changed the intra- and inter-areal spatial summation relationships (Fig. 6d). With the smaller skin surface area represented by a millimeter of cortex in BA3b than BA1, the skin representation of intrinsic connections tended to be larger in BA1 than in BA3b. However, in BA1 two of the three cases showed similar skin coverage of the intrinsic connections to that found in BA3b and the larger value was a result of a single case with an extremely large kernel area size (Fig. 6c, d). Again, more cases are needed to clarify this discrepancy. Regarding inter-areal connections, feedback from BA1 exhibited significantly larger skin size representation than that of feedforward projection from BA3b (two-tailed t-test, $p = 0.01$). Also, for BA3b the skin representation of feedback connections from BA1

was nearly equivalent to the skin representation of the intrinsic connections. In contrast, for BA1 the skin representation of intrinsic connections was greater than the feedforward connections from BA3b. Interestingly, within an area intrinsically projecting neurons provided spatial summation from a larger patch of skin than inter-areal projection neurons.

Relationship of the distribution of projection neurons and the OIS-area of activation

Proportion of neurons within the OIS: To examine the spatial relationship of connections projecting to an injection site with the size of the cortical population receptive field (pRF), we evaluated the ratio of the number of labeled neurons within an OIS-area following stimulation of the distal finger-pad relative to the total number of labeled neurons within the corresponding cortical area (i.e. either BA3b or BA1, Fig. 6e). Figure 6b shows that a considerable proportion of retrogradely labeled neurons were localized within the representation of a distal finger pad. Examination of the ratios revealed that with a BA3b injection the majority of the intrinsic projecting neurons were located within the cortical pRF of the injected finger pad; in contrast, a much lower proportion of inter-areal feedback neurons overlapped with the evoked OIS-area in BA1. On the other hand, with a BA1 injection, only a low proportion of intrinsic neurons were located within the OIS-area; in comparison, inter-areal feedforward neurons showed a higher overlap with the OIS-area in BA3b. It should be noted that the OIS-area largely overlapped with the highest kernel density area in all cases except case P where the injection site felt outside of the OIS-area (Fig. 2). However, due to the steep decline of retrograde labeling density a small injection offset from the targeted OIS-area would result in a relatively large difference in the percentage of the projection neurons localized within the corresponding OIS-area. We should note that consistent with the CMF difference, the OIS-area sizes were different for BA3b and BA1 which could have contributed to the lower proportion of neurons located in the OIS-areas of BA1. We should also note that the OIS-areas for BA1 were obtained under anesthesia, and since anesthesia is known to affect higher cortical areas to a greater extent than primary sensory areas (Chen et al. 2005) the OIS-areas are likely an underestimate of cortical pRFs for BA1. Since the mapping studies were performed under anesthesia, these percentages therefore can be considered as underestimations.

Relative spread of the high density labeling and the OIS: To further explore the spatial relationship of connections projecting to an injection site (as in Fig. 6a, b), we specifically examined the size of the highest density of retrograde labeling. In this particular comparison kernel density maps were computed separately for the intra- and inter-areal labeling. This procedure allowed exploration of the fine structure of labeling density, in this case the demarcation of the highest density regions of inter-areal labeling, and its potential role in intra- and inter-areal cortical communication without the bias of the overwhelmingly high intra-areal labeling density (Fig. 2). As shown in Table 1 the size of the peak densities were similar for both the intra- and inter-areal labeling. The following tendencies were also observed. For BA3b injections the intra-areal size of the highest density region of the projection neurons was only slightly larger than the inter-areal size; whereas, for BA1 injections the inter-areal spread was larger than the intra-areal spread. Please note, however, that both for the intra-areal and inter-areal labeling the sizes of the highest density of

neuronal labeling tended to be smaller in BA1 than in BA3b, suggesting that the size of the spread of the projection neurons could be related to the smaller CMF of BA1 than that of BA3b. Consequently, we examined the size of the peak densities after taking into account the CMF differences between the two areas (Table 1). With a BA3b injection, the highest density of intrinsic neuronal projections represent a much more focal patch of skin than that of the highest density region of the inter-areal feedback connections from BA1. With a BA1 injection, the highest density of intrinsic neuronal projections represent a much larger area of skin than found in case of the feedforward projections from BA3b.

Whether the highest density of neuronal projections was related to the pRF was investigated by comparing the size of the highest density retrograde labeling to the OIS-area. As shown in Figure 6f, the size of the highest density of neuronal projections was comparable to the area of activity elicited by digit stimulation; the highest density kernel-area/OIS-area ratios were around 1. The only exception appeared to be the spread of the intrinsic connection of BA1, which in average was about twice the size of the OIS-area. However, comparisons using one sample t-test showed that the ratios did not significantly differ from 1 in any of the connections studied. In contrast to the observed total neuronal number/OIS-area ratios (Fig. 6e), which suggest different intrinsic and inter-areal relationships between BA3b and BA1, this finding supports that the highest density of neuronal input is from homologous cortical pRFs. There were weak trends for the highest density kernel-area/OIS-area ratios to be larger with BA1 injections for intrinsic than for feedforward projections from BA3b; whereas with BA3b injections the ratios were smaller for the intrinsic than for the feedback projections from BA1 (two way, repeated measure ANOVA, $p = 0.09$). These trends were likely a consequence of the smaller OIS-areas for BA1. Again we should note that since the OIS-areas were obtained under anesthesia, these are likely underestimates of cortical pRFs, especially for BA1.

5. Lateral spread of the anterograde labeling

The distribution of axonal patches was measured (1) by determining the cortical area covered by a patch group (patch group size), (2) by computing the distance between patches within a cortical area, as a measure of patch packing density, and (3) by calculating the radial distance of patches either from the injection site (intra-area) or from the center of mass of the highest kernel density area (inter-area), as a measure of cortical spread.

Size of axonal patch groups—To evaluate the cortical area covered by an axonal patch group we first determined the size of the individual groups of patches (patch group size). Patch group area is the sum of the non-overlapping regions of the individual patches plus the area formed by overlapping patches after merging the sections. The size of the cortical region covered by the groups of patches was different for the injections in BA3b and BA1. Patch group sizes were larger after an injection in BA1 than in BA3b (Fig. 7a). Patch group size also were larger for inter-areal projections than intrinsic projections (one-tailed t-test, $p = 0.01$), supporting that, in general, the modulation by intrinsic efferents is more spatially confined than inter-areal efferents. In BA1 intrinsic and inter-areal cortical coverage of the patch groups were similar, but in BA3b the size of the intrinsic patch group was much smaller than those projecting from BA1.

By converting cortical coverage into represented skin size, after considering the CMFs of BA3b and BA1, a different picture emerges especially for the BA1 efferents (Fig. 7b). With a BA1 injection the patch group of intrinsic efferents covered a larger patch of skin than that of the feedback efferents to BA3b (one-tailed t-test, $p = 0.03$). Furthermore, larger patches of skin were covered by the inter-areal feedforward than the feedback efferent patches. Both of these findings were opposite to that found when only the cortical size of the patch groups was considered. However, some of these conclusions require further supporting evidence, as for the feedforward patch groups the relatively large average size was a result of a single case with a large deviation from the other two cases (Fig. 7b). On the other hand, similar to cortical size, the patch of skin encompassed by an axonal patch group of intrinsic efferents was smaller for BA3b than BA1. Furthermore, for a BA3b injection a patch group of intrinsic efferents encompassed a much smaller patch of skin than that of the feedforward efferents to BA1.

To investigate the functional relationship of the patch groups and the cortical population response, the size of the patch groups (Fig. 7a) and the OIS-area were compared in BA3b and BA1. With the exception of intrinsic connections of BA3b the ratios of patch group-area/OIS-area were centered around 1 showing nearly equivalent sized patch groups with OIS-areas (Fig. 7c). Only the small intra-areal ratio of BA3b differed significantly from 1 (one sample t-test, $p = 0.003$). With the BA1 injection the ratio of about 1 implies BA1 efferents target the full cortical pRF of the distal finger pad in both BA3b and BA1; whereas after a BA3b injection a ratio of less than 1 indicates that intrinsic patch groups of BA3b efferents target a more focal region of the cortical pRF of the distal finger pad in BA3b.

Lateral spread of axonal patches—Evaluation of the packing density of the axonal patches, which can be considered as a measure of spatial dispersion vs. summation was measured by using the nearest neighbor function of Neurolucida Explorer. The nearest neighbor function calculated the average distance between nearest patch groups, where shorter distances between patch groups would indicate a greater packing density (Fig. 8a). As shown in Figure 8c, irrespective of whether the efferents were intrinsic or inter-areal, the packing density of the patch groups was greater after BA3b than BA1 injection. These findings indicate BA1 exhibits a larger dispersion of the efferents than BA3b, which was independent of whether the efferents were intrinsic, feedforward or feedback.

The spatial dispersion of the axonal patches was also evaluated based of their distances from a center point (the injection site in case of intra-areal labeling; the center of mass of the highest kernel density area in case of inter-areal labeling) (Fig. 8b). In contrast to the packing density, this measure of the efferents is related to the spatial divergence, i.e. the distribution of information from a predetermined cortical site. The average patch distances from a center point were larger for intra-areal than the inter-areal patches (for BA3bij the difference was significant: one-tailed t-test, $p = 0.03$); and for inter-areal labeling the feedback patch groups after BA1 injections exhibited larger spread than the feedforward projections after injecting BA3b (Fig. 8d). A different relationship was observed after considering the CMFs and converting the cortical spread of the axonal patches into average distances along the surface of the skin (Fig. 8e). For BA3b, patch distances were similar for intrinsic and inter-areal efferents; whereas, for BA1 patch distances were much larger for the

intrinsic connections than the inter-areal feedback connections with BA3b (one-tailed t-test, $p = 0.01$). In addition, the spread of intrinsic axonal patches represented significantly larger the skin size in BA1 than in BA3b (two-tailed t-test, $p = 0.02$).

6. Direct comparisons of the spread of projection neurons and efferents

To directly relate the cortical spread of axonal patches emanating from a cortical locus with that of the neuronal population projecting to that site, we compared the distance of the patches (Fig. 8d) with a corresponding measure of the radius of the highest kernel density area (Table 1) to obtain a ratio of axonal patch/neuron spread (Fig. 8f). This ratio quantifies whether a cortical site sends efferent projections within its most effective (highest density) input region, which corresponds well to the pRF (see Fig. 6f), or provides input to cortical regions that are either smaller or larger. As shown in Figure 8f, the intra-areal ratio was significantly greater than the inter-areal ratio (two way, repeated measure ANOVA, $p = 0.01$; post-hoc comparison: one-tailed t-test, $p << 0.01$). Within BA1 the inter-areal ratio was very low (the smallest value on Fig. 8f) in contrast to the high value of intra-areal ratio (the largest value on Fig. 8f). In contrast to BA1, both the intra and inter-areal ratios tended to be closer to 1 within BA3b. However, irrespective of the injected area, neither the intra-areal nor the inter-areal ratio appeared larger than 1, the difference was not significant at the 95% confidence level (one sample t-test). Also, the ratios appeared larger after BA1 than after BA3b injections the difference was not statistically significant as indicated by the lack of significant interaction in two way, repeated measure ANOVA ($p = 0.94$).

To further investigate the spatial relationship between the reciprocal intrinsic and inter-areal feedback and feedforward connections the patch groups were counted for the full range of kernel density regions after aligning the two maps (Fig. 9a, b). Kernel densities of the neuronal projections were ranked beginning with the highest value of the intra-areal or inter-areal labeling where there was an overlapping with the patch groups. The distribution of kernel densities found at locations with terminal patch groups revealed that intra-areal axonal patch groups spread over a larger range of neuronal labeling densities than inter-areal patch groups (Fig. 9c, d). Furthermore, axonal patches labeled by BA3b injection were concentrated more in regions of high density neuronal labeling while that of BA1 showed a larger dispersion towards lower density regions of neuronal labeling both for intra-areal and inter-areal connections. Consequently, as shown in Figure 9d inter-areal feedforward efferents in BA1 targeted regions of higher density neuronal labeling than feedback axonal patches which targeted territories with lower retrograde labeling densities in BA3b.

7. Oriented connectional distribution within and between the areas

Anisotropy of the distribution of projection neurons and efferent axonal patches—The extent of connectional anisotropy and its orientation determines the major direction of neural interactions on the topographic, in our case somatotopic map. The anisotropic distribution of the anterogradely labeled axonal patches and retrogradely labeled projection neurons (Fig. 1a, C; Fig. 2) was tested and compared after computing the anisotropy index of Sinchich and Blasdel (2001) (Fig. 10a, d). In all cases the anisotropy index (r) was larger than zero for both neuronal structures (Fig. 10b, e). However, in case of the projection neurons only the anisotropy index of the feedback deviated significantly from

zero at 95% confidence level (one sample t-test). On the other hand, in case of the axonal patches all pathways except the intra-areal patches of BA1 differed significantly from zero at 95% confidence level. Comparisons showed larger anisotropy of the spread of efferent axonal patches than that of projection neurons (two way, repeated measure ANOVA, $p = 0.001$). Post hoc comparisons supported that axonal patches showed a greater anistropic distribution than projection neurons only for the inter-areal labeling (one-tailed t-test, $p < 0.01$). Note that some of the difference observed may be a consequence of the analysis where for the projection neurons each labeled element (neuron) was included into the examination whereas for the axonal patches only the clusters of the highest labeling bouton densities were included.

The orientation of the elliptical spread of projection neurons and efferent patches was studied by measuring the angle between the anisotropy vectors and the border of BA3b and BA1, which is roughly parallel with the hand representation across the fingers. Consequently 0° degrees would indicate that the labeling was distributed equally across the finger representations whereas a degree of 90° would indicate that the labeling was distributed perfectly along the proximal to distal axis of the finger representation and palm region (Fig. 10a, c, d, f). For most instances, the distribution of neurons and axonal patches was oriented across the representation of the fingers (Fig. 10c, f; < 45 degrees). It should be noted that the inter-areal efferent patches within BA1 were spatially highly restricted suggesting this anisotropy and the relatively high angle (> 45 degrees) is a local effect within the distal finger pad region (Figs. 1, 2) (see also Négyessy et al. 2013). Multiple comparisons using factorial ANOVA did not resulted in significant differences between the orientation angles of the intrinsic, feedforward and feedback connections.

Distribution of the fast conduction pathways—Finally, we found an interesting relationship between the anisotropic distribution of the intra- and inter-areal labeling and the orientation of BDA labeled, horizontally running thick and smooth axonal fibers. These thick axon-like processes (Fig. 11a) were found both in the supra- and infragranular layers. We assumed that they represent, at least in part, myelinated axons, which are responsible for fast activity propagation. Accordingly, using electron microscopy we found tangentially cut BDA labeled myelinated axons both in BA3b and BA1 irrespective of the site of injection and the layers studied (Fig. 11d). Notably, mapping the labeled thick axon-like processes suggested that they form connections mostly between the areas rather than within the areas (Fig. 11b, e). In order to identify the prevalent direction of the orientation of the reconstructed labeled processes the maps of the different cases were overlaid and then plotted in a polar diagram. In Figure 11c and f the black color representing the overlap between the cases indicated that the axon-like thick processes run predominantly between the areas rather than within the areas. This pattern of labeling exhibited an apparently orthogonal orientation to that of the anterograde and retrograde labeling within BA3b and BA1 as shown by the anisotropy analyses (compare Figs. 2a, d, Fig 10, and Fig. 11c, f).

Discussion

Circuitry of columnar interactions within and between BA3b and BA1

In this study we compared the lateral spread of inputs (projection neurons) and targets (efferent axonal patches) of column size cortical sites in the distal finger pad representations of the reciprocally connected and hierarchically organized somatosensory cortical areas 3b and 1. The analysis focused on the regions with high connectional densities, low density, more diffuse connections were not studied here. Several hierarchically relevant characteristics of the anatomical basis of lateral cortical interactions were explored, which were not studied before in the SI, by comparing the spread of intrinsic, feedforward and feedback connections. Most notably we found that, similarly to the visual cortex (Angelucci and Bressloff 2006; Markov et al. 2014), the lateral spread of the feedforward connections are the most restricted and can form the connectional basis of receptive field hotspots in SI (Favorov and Whitsel 1988) (Figs. 6, 7, 8, 9). On the other hand, the large lateral spread of the feedback and intrinsic connections suggest their role in the formation of the ecRF and, more generally, in tactile integrative processing in SI (Figs. 6, 7, 8, 9). We also show that although the cortical spread of intrinsic connections is not remarkably different in BA3b and BA1, the smaller CMF results in a more widespread spatial integration of the peripheral input from the skin in BA1 than in BA3b (Figs. 6c, d, 8d, e). The spread of the intra-areal feedforward and feedback connections relative to the OIS-area also reveals that these connections contribute to the cortical population response (Figs. 6e, f, 7c, 8f). We also show, for the first time, that similar to the intrinsic connections feedforward and feedback are also anisotropically distributed across the finger representations (Fig. 10). Regarding the dynamics of interactions, the results show the existence of a fast conducting inter-areal pathway (Fig. 11), similar to what have been described in the visual cortex (Angelucci and Bressloff 2006). These observations have led us to modify our previous model of the circuitry of BA3b and BA1, where we proposed that there is a larger spread of the intrinsic than the inter-areal connectivity (Négyessy et al. 2013; Wang et al. 2013; Ashaber et al. 2014). In contrast, this study shows that in BA3b feedback efferent axonal patches originating from BA1 spread to a similar extent as the intrinsic ones (Fig. 8d). Taken all together, the comparative analyses of the circuitry obtained by the injection of two reciprocally connected areas provides fundamental information about the canonical connectional motif of information exchange in a network of cortical areas. The present discoveries concerning somatosensory cortical connectivity are summarized in Figure 12.

Please note the differences of Figure 12 and the summary diagram of Wang et al. (2013, Figure 8). One of the major difference is a consequence that the findings of Wang et al. (2013) were based on the observations made after injecting BA3b only. Accordingly, a noticeable difference is the presence of feedback in Figure 12, which now can be included by using the data obtained by BA1 injections. A further novelty in Figure 12 is the representation of a pathway consisting of fast conducting axons. Finally, Figure 12 also shows the different clustering of the projection neurons in the two areas, which has not been examined in our previous studies.

Pitfalls and weaknesses

The small sample size is a noticeable weakness of our comparisons. This is a general problem with primate studies where a limited case number is compensated by the collection of complementary data sets. Accordingly, the power of the statistical comparisons where performed could not be sufficiently strong. In any case, the quantitative measures supported the qualitative observations. As an example, by looking at Figure 2 at the spread of retrograde and anterograde labeling, one can notice the lower densities and smaller territories occupied by the inter-areal labeling compared to the intra-areal labeling, which agrees with the quantitative data shown on Figures 6c, d and 8f. Also, except for some cases that appear as outliers, the different measures were consistent across cases (see the slant of the lines on Figs. 6, 8 and 10). Large deviations appeared in the raw measurements (area, length) and reflect the sensitivity of these values to the inherent variability of anatomical tracer studies, to sampling (Vezoli et al. 2004) and to individual differences present normally in the population. It should be noted that there are caveats in making direct comparisons across different anatomical structures (for instance, generating equivalent measures for the spread of efferent patches and projection neurons). Still these comparisons provide an opportunity to make inferences about the relationships between the intrinsic and inter-areal connections of these 2 hierarchically organized cortical areas. Using relative quantities (ratios) helped with these issues and also increased consistency of the data across cases.

Another weakness regards our laminar analyses of the distribution of the BDA labeling. Our approach did not allow for the determination of the exact laminar distribution of labeling because of the loss of data during sampling of the tangentially cut series of sections. The exact laminar distribution can be defined only from complete series or coronal sections. Still, we were able to discern a high ratio of supragranular labeling that is in accordance with the literature (Burton and Fabri 1995), although a higher proportion of infragranular labeling is reported than in the present study. The prevalence of supragranular labeling in these two neighboring low level somatosensory areas is also in agreement with the pattern seen in hierarchically organized visual cortical areas (Barone et al. 2000; Vezoli et al. 2004).

Hierarchical features of the lateral spread of somatosensory cortical connections

Lateral spread of connections—Connectional hierarchy of the cerebral cortex is mostly defined by laminar distributional properties; in contrast, the hierarchical features of the horizontal spatial spread of the connections is less well known (Angelucci and Bressloff 2006; Markov et al. 2013, 2014). The present study provides evidence, complementing earlier findings in visual cortex (Angelucci and Bressloff 2006; Markov et al. 2014), that feedback projection neurons and efferent axonal patches have a larger lateral spread and thereby integrate information over a larger skin area than feedforward connections.

Our analyses found that in BA3b the feedback afferent axonal patch groups from BA1 have a larger cortical spread than the high density intra-areal input from projection neurons. Contrary to that, within BA1 intrinsically projecting neurons have larger spread than the feedforward afferent axonal patch group from BA3b. It was also shown that the high density region of intrinsically projecting neurons matches the size of the OIS-area. These observations indicate that feedforward afferents target the OIS-area of population activity

with homologous somatotopic representation while feedback afferents reach heterologous somatotopic representations, which is in agreement with the findings of Juliano et al. (1990). The heterologous somatotopic localization of the feedback efferent axonal patches suggests their contribution to ecRF properties in SI, similar to what is observed in visual cortex (Angelucci and Bressloff, 2016). The large spatial spread of the feedback axonal patches was accompanied by a low packing density and an increase in the frequency of targeting lower density regions of the projection neurons. These observations are consistent with the modulatory role of feedback in contrast to the highly convergent and driving-like effects of feedforward connections (Angelucci and Bressloff 2006; Markov et al. 2013, 2014). Notably, Angelucci et al. (2002) also showed that in V1 the lateral spread of feedback becomes more extensive with the greater hierarchical distance from V1. Similarly, in BA3b feedback from a higher cortical level than BA1 (e.g BA5, Pearson and Powell 1978; Burton and Fabri 1995) could have a larger lateral spread exceeding not only the spread of the BA1 feedback patches but also the highly dense intrinsically projecting efferent patches. This feedback circuitry can be responsible for surround interactions in the neuronal receptive fields of somatosensory cortex, similar to that found in visual cortex (Angelucci and Bressloff 2006). These observations refine our previous suggestion emphasizing the role of intrinsic connections in lateral interactions by complementing it with feedback projections in SI (Wang et al. 2013).

Calculating the skin coverage of these neural connections with the help of the CMF made clear that BA1 integrates considerably larger peripheral input than does BA3b. This was found for the intrinsic connections as well as for the feedback projection neurons localized in BA1. Interestingly, in BA3b the represented skin size of the feedback axonal patches, which exhibits a relatively large spread in terms of cortical distance, is only about the same as that represented by the spread of the intrinsic efferents of BA3b. By considering the relatively large skin coverage of the population of the feedback projection neurons, these observations indicate that the feedback patches convey heterologous somatotopic information into BA3b. In agreement with the large, multifinger RFs and the complex RF properties of BA1 neurons these observations suggest that in BA1 lateral cortical interactions allow more extensive peripheral integration than those in BA3b (Sathian 2016; Yau et al. 2016).

Clustering of projection neurons—One of the interesting findings of our study was the different spatial grouping of the projection neurons in BA3b and BA1. Larger number of clusters were found in BA3b than in BA1, which indicate an increased propensity of grouping of the projection neurons in BA3b. A careful examination of the figures presented in studies on the distribution of visual cortical projection neurons within and between areas suggests that, similarly to our observations in SI, the connectional distributions are more tightly clustered in V1 than in V2 (Gilbert and Wiesel 1989; Jeffs et al. 2009; Negwer et al. 2017). Interestingly, using double retrograde tracing Markov et al. (2014) showed that in visual cortex inter-areal projection neurons exhibit higher topographic specificity, i.e. a more spatially concentrated distribution, in the supragranular layer than in the infragranular layer. However, the high supragranular ratio (Fig. 4b) and the similar clustering of both the intrinsic and inter-areal projection neurons in the two areas make it unlikely that our finding

is a result of different laminar clustering of the projection neurons. Instead, at least in part, our observations could be related to the cell density differences in the two areas; where BA3b is known to have a higher density than BA1 (Sur et al. 1982). However, in spite of the high neuronal density in BA3b inter-areal and intra-areal labeling densities did not differ following BA1 injection to the extent seen after injection of BA3b (Fig. 2). The larger difference between the densities of the intra- and inter-areal neurons projecting to BA3b compared to the projection to BA1 can be a result of the labeling in the granular layer, which is mostly responsible for the elevated neuronal density of BA3b (Sur et al. 1982). Accordingly, the granular layer is formed predominantly by local circuit neurons labeled by the tracer injection in this area. The observation that the number of intra-areal and inter-areal clusters exhibited a considerably larger difference following BA3b than after BA1 injections is consistent with the role of the granular layer in the increased grouping of the projection neurons of BA3b. However, clustering of the inter-areal projection neurons, which originate mostly from the supraganular layers, is also higher in BA3b than in BA1, suggesting that neuronal density differences of the granular layer can only partially explain the difference seen in the number of clusters in the two areas. Considering these observations our findings are consistent with the suggestion of Herculano-Houzel et al. (2008) that, based on the non-uniform density of neurons across the cortical areas, columns of different areas have different density of inter-areal connections.

An interesting possibility for the variable grouping of the connections in the different areas is that clustering and RF size are interrelated, resulting in a higher clustering propensity of neurons with smaller RFs as seen in BA3b where neurons have small RFs compared to that in BA1 (Iwamura et al. 1983a; Sur et al. 1980, 1985). Considering the topographic organization of the connectivity and the higher density of the projection neurons, the stronger clustering could lead to some of the tactile hyperacuities in BA3b (Mancini et al. 2012). On the other hand, one can speculate that in higher order areas the lower clustering of the connections results in a sparse sampling from the relevant functional maps. A major question is whether such sparse sampling is related to receptive field size and complexity as in BA1 where neuronal RFs exhibit larger complexity and more nonlinearities than in BA3b (Iwamura 1998; Sripati et al. 2006). The present observations suggest clustering of projection neurons can be a hierarchically relevant feature of cortical connectivity in line with earlier findings pointing to a relationship between hierarchy, connectivity, functional representation and cytoarchitecture (i.e. cell density) of cortical areas (Dombrowski et al. 2001; Hilgetag and Grant 2010; Barbas 2015; Barbas and García-Cabezas 2016; Hilgetag et al. 2016).

Connectional basis of ecRF in SI

The lateral spread of the connections found in this study (discussed in detail above) is consistent with observations in the visual cortex showing that feedforward connections form the RF center while intrinsic and feedback connections are largely responsible for the surround organization including the ecRF (Girard et al. 1989; Bullier et al. 1996; Hupé et al. 1998; Bair 2005; Angelucci and Bressloff 2006; Harrison et al. 2007; Bardy et al. 2009). The anisotropic distribution of the connections adds further functionally relevant observations regarding the role of intrinsic and inter-areal connections in RF organization

similarly as shown in the visual cortex (Sinchich and Blasdel, 2001). That intra-areal connections are anisotropic and mediolaterally oriented provides quantitative support for our previous observations on multidigit integration within BA3b and BA1 (Négyessy et al. 2013; Ashaber et al. 2014; Wang et al. 2013). Furthermore, with a lesser degree inter-areal connectivity is also anisotropic and exhibits a similar mediolateral distribution. The similar orientation of projections suggests that the lateral extent of the distribution of intrinsic and inter-areal connections determines their role in the spatial integration in SI. These observations indicate that integration across finger representations is a primary function of the BA3b and BA1 circuitry, including not only intrinsic connections as suggested before (Négyessy et al. 2013; Ashaber et al. 2014; Wang et al. 2013) but inter-areal connectivity as well.

An additional important observation of the present study was the spatially restricted, topographically organized reciprocal connection formed by thick axons between the homologous distal finger pad representations of BA3b and BA1. The smooth light microscopic appearance of these thick axons, together with the electron microscopic analysis suggest that these axons may be myelinated. However, a direct proof of the myelination of the thick, inter-areal axons requires intracellular labeling combined with electron microscopy and/or double labeling. Nevertheless, in agreement with observations in visual cortex (Angelucci and Bressloff 2006), our findings show that feedforward as well as feedback pathways consist of fast conductive axons allowing highly dynamic inter-areal communication. In V1 the high velocity inter-areal pathways result in the short latency modulation of both the center and surround receptive fields (Angelucci and Bressloff 2006). The quick information exchange between BA3b and BA1 allows rapid updating of the processing between the cortical regions sharing the same pRFs. However, because of the restricted lateral spread of the thick axons as shown here, further studies are needed to explore the physiological relevance of a fast conducting inter-areal pathway in regard to RF properties in SI.

Our results can speak to the submodality integration at the level of single cell receptive fields of BA3b. Pei et al. (2009) showed that in BA3b a significant proportion of neurons exhibit both slowly (SA1) and rapidly adapting (RA1) responses. The authors proposed that the mixed receptive field response was due to the convergence of different mechanoreceptors via the thalamocortical input to BA3b (Pei et al. 2009). However, given the stimulus durations (≥ 62 ms) and delay times (≥ 100 ms) between the stimuli and the neuronal responses, the findings suggest that in addition to the thalamic input, cortical interactions may be responsible for the described effects. The reciprocal fast conducting pathway described in this study can quickly transfer BA1 responses, where RA1 is abundant (Paul et al. 1972), to BA3b. In this context, it is interesting to note that the RA1 characteristics appeared relatively late as an OFF response in the evoked activity of area 3b neurons with mixed submodality response properties (Pei et al. 2009). Another explanation can be the interaction of the submodality modules within BA3b via intracortical circuitry (Sur et al. 1981; Chen et al. 2001; Reed et al. 2010a,b). Similar modular representation of RA1, SA1 and Pacinian channels was described in BA1 (Friedman et al. 2004), which provides even further possibilities for their integration via iterative intra-areal and inter-areal interactions, akin to the cortical integration motif suggested by Rockland (2015).

Anatomical foundations of the cortical population response

The present study also shows that the lateral spread of afferent inputs (projection neurons) and targets (efferent axonal patches) of a column-sized cortical site varies and depends on the cortical area and its position in the hierarchical organization of cortical connectivity. In humans fMRI observations suggest that the size of pRFs in neighboring visual cortical areas is dependent on both the CMF and the size of the cortical area activated in primary sensory cortex, and not on eccentricity (Harvey and Dumoulin 2011). In the present study pRF size represented by the OIS-area was matched very well by both the spread of the intrinsically projecting neurons and, except for the intrinsic connections of BA3b, the individual efferent axonal patch groups. Similar to the finding in V1, where the pRF is inversely related to eccentricity (Harvey and Dumoulin 2011), the OIS-area varied according to the CMF and was larger in BA3b than in BA1, in agreement with previous observations in somatosensory cortex (Friedman et al. 2008). Consequently, for both afferent and efferent labeling there was an overall tendency for larger skin size representations in BA1 than in BA3b just as shown for the visual cortical pRF size, which increases with decreasing CMF (Harvey and Dumoulin 2011). Our observations about the lateral spread of the connectivity refine the suggestion from the fMRI data (Harvey and Dumoulin 2011) by showing that the size of tissue involved in cortical interactions could vary depending on the area and hierarchical relationship studied. Furthermore, based on their similar sizes, the interactions of the high density projection neurons with the overlapping efferent patch groups can form the anatomical basis of the population response in the cerebral cortex. The size of the activated cortical site can be further enlarged by intrinsically projecting and feedback efferent axonal patches via their large lateral spread especially in the awake condition (Chen et al. 2005). Considering that a similar connectional architecture is responsible for the visual cortical RF properties including the ecRF (Angelucci and Bressloff, 2006) and that modular organization of the connections appears to be a general feature of the primate cerebral cortex (Lund et al. 2003), the present analyses of the column based circuitry of two neighboring interconnected areas suggest there is a common connectional motif of cortical processing at the mesoscale population level.

Such a canonical model is built on the following features: a column size of cortical tissue receives high density intra-areal input from projection neurons with a lateral spread expanding through the termination area of the feedforward input from a lower level area, which determines the classical RF of the neurons. In contrast, high density inter-areal feedforward and feedback neurons projecting to a column of a neighboring area exhibit more restricted lateral spread and therefore is formed either by a subset of the intrinsically projecting neurons or by a different set of projection neurons probably in the core of the high density intra-areal input region. Regarding inter-areal axonal terminations, feedforward patches overlap with the feedforward and feedback neurons projecting to a column of a neighboring area. In contrast feedback axonal patches originating from a neighboring area distribute more widely, reaching distant cortical regions outside of the high density intrinsically projecting neurons, similar to the intrinsic axonal patches. However, the size of the spread of the feedback patches increases with the hierarchical distance between the target area and the area of origin. Therefore intrinsic and feedback efferent axonal patches play important role in determining the ecRF. Finally, connections distribute anisotropically,

or at least exhibited a tendency for it, relative to the topographic representation of the area. Also, projection neurons exhibit higher clustering in lower than higher order areas while intrinsic axonal patches of lower order areas and feedforward axonal patches exhibit stronger clustering than the feedback and the intrinsic patches of higher order areas. This model is depicted in Figure 12.

Acknowledgements

Supported by the Fogarty International Research Collaboration Award, U.S. National Institutes of Health; Grant numbers: NS059061 (to A.W.R. and L.N.), NS044375 and NS093998 (to A.W.R.) as well as the Hungarian Scientific Research Fund; Grant number: OTKA NN79366 (to L.N.).

1)(in case of Funding) Funding:

o Fogarty International Research Collaboration Award,NS059061 (to A.W.R. and L.N.),

o U.S. National Institutes of Health NS044375 and NS093998 (to A.W.R.)

o Hungarian Scientific Research Fund; Grant number: OTKA NN79366 (to L.N.)

References

Angelucci A, Bressloff PC (2006) Contribution of feedforward, lateral and feedback connections to the classical receptive field center and extra-classical receptive field surround of primate V1 neurons. Prog Brain Res 154:93–120 [PubMed: 17010705]

Angelucci A, Levitt JB, Walton EJ, Hupe JM, Bullier J, Lund JS(2002) Circuits for local and global signal integration in primary visual cortex. J Neurosci 22:8633–46 [PubMed: 12351737]

Ashaber M, Pálfi E, Friedman RM, Palmer C, Jákli B, Chen LM, Kántor O, Roe AW, Négyessy L (2014) Connectivity of somatosensory cortical area 1 forms an anatomical substrate for the emergence of multifinger receptive fields and complex feature selectivity in the squirrel monkey (Saimiri sciureus). J Comp Neurol 522:1769–85 [PubMed: 24214200]

Bair W (2005) Visual receptive field organization. Curr Opin Neurobiol 15:459–64 [PubMed: 16023850]

Barbas H (2015) General cortical and special prefrontal connections: principles from structure to function. Annu Rev Neurosci 38:269–89 [PubMed: 25897871]

Barbas H, García-Cabezas MÁ (2016) How the prefrontal executive got its stripes. Curr Opin Neurobiol 40:125–134 [PubMed: 27479655]

Bardy C, Huang JY, Wang C, Fitzgibbon T, Dreher B (2009) 'Top-down' influences of ipsilateral or contralateral postero-temporal visual cortices on the extra-classical receptive fields of neurons in cat's striate cortex. Neuroscience 158:951–68 [PubMed: 18976693]

Barone P, Batardiere A, Knoblauch K, Kennedy H (2000) Laminar distribution of neurons in extrastriate areas projecting to visual areas V1 and V4 correlates with the hierarchical rank and indicates the operation of a distance rule. J Neurosci 20:3263–81 [PubMed: 10777791]

Bullier J, Hupé JM, James A, Girard P (1996) Functional interactions between areas V1 and V2 in the monkey. J Physiol Paris 90:217–20 [PubMed: 9116670]

Burton H, Fabri M (1995) Ipsilateral intracortical connections of physiologically defined cutaneous representations in areas 3b and 1 of macaque monkeys: projections in the vicinity of the central sulcus. J Comp Neurol 355:508–38 [PubMed: 7636029]

Buzás P, Kovács K, Ferecskó AS, Budd JM, Eysel UT, Kisvárday ZF (2006) Model-Based Analysis of Excitatory Lateral Connections in the Visual Cortex. J Comp Neurol 881:499–861

Chen LM, Friedman RM, Ramsden BM, LaMotte RH, Roe AW (2001) Finescale organization of SI (area 3b) in the squirrel monkey revealed with intrinsic optical imaging. J Neurophysiol 86:3011–3029 [PubMed: 11731557]

Chen LM, Friedman RM, Roe AW (2003) Optical imaging of a tactile illusion in area 3b of the primary somatosensory cortex. Science 302:881–885 [PubMed: 14500850]

Chen LM, Friedman RM, Roe AW (2005) Optical imaging of SI topography in anesthetized and awake squirrel monkeys. J Neurosci 25:7648–59 [PubMed: 16107651]

Cleland TA (2010) Early transformations in odor representation. Trends Neurosci 33:130–13910 [PubMed: 20060600]

Costanzo RM, Gardner EP (1980) A quantitative analysis of responses of direction-sensitive neurons in somatosensory cortex of awake monkeys. J Neurophysiol 43: 1319–1341 [PubMed: 6768849]

Dombrowski SM, Hilgetag CC, Barbas H (2001) Quantitative architecture distinguishes prefrontal cortical systems in the rhesus monkey. Cereb Cortex 11:975–88 [PubMed: 11549620]

Ester M, Kriegel H, Sander J, Xu X (1996) A Density-Based Algorithm for Discovering Clusters in Large Spatial Databases with Noise. KDD-96 Proceedings 34:226–31

Favorov O, Whitsel BL (1988) Spatial organization of the peripheral input to area 1 cell columns. I. The detection of “segregates”. Brain Res 472:25–42 [PubMed: 3342334]

Federer F, Delaney W, Ichida JM, Merlin S, Angelucci A (2013) Two Projection Streams from Macaque V1 to the Pale Cytochrome Oxidase Stripes of V2. J Neurosci 33:11530–39 [PubMed: 23843523]

Felleman DJ, Van Essen DC (1991) Distributed hierarchical processing in the primate cerebral cortex. Cereb Cortex. 1:1–47. [PubMed: 1822724]

Friedman RM, Chen LM, Roe AW (2004) Modality maps within primate somatosensory cortex. Proc Natl Acad Sci USA 101:12724–12729 [PubMed: 15308779]

Friedman RM, Chen LM, Roe AW (2008) Responses of areas 3b and 1 in anesthetized squirrel monkeys to single- and dual-site stimulation of the digits. J Neurophysiol 100:3185–96 [PubMed: 18922955]

Gilbert CD, Wiesel TN (1989) Columnar specificity of intrinsic horizontal and corticocortical connections in cat visual cortex. J Neurosci 9:2432–42 [PubMed: 2746337]

Girard P, Bullier J (1989) Visual activity in area V2 during reversible inactivation of area 17 in the macaque monkey. J Neurophysiol 62:1287–302 [PubMed: 2600626]

Hackett TA, de la Mothe LA, Camalier CR, Falchier A, Lakatos P, Kajikawa Y, Schroeder CE (2014) Feedforward and feedback projections of caudal belt and parabelt areas of auditory cortex: refining the hierarchical model. Front Neurosc 8:72

Harrison LM, Stephan KE, Rees G, Friston KJ (2007) Extra-classical receptive field effects measured in striate cortex with fMRI. Neuroimage 34:1199–208 [PubMed: 17169579]

Harvey BM, Dumoulin SO (2011) The relationship between cortical magnification factor and pRF size in human visual cortex: constancies in cortical architecture. J Neurosci 31:13604–12 [PubMed: 21940451]

Herculano-Houzel S, Collins CE, Wong P, Kaas JH, Lent R (2008) The basic nonuniformity of the cerebral cortex. Proc Natl Acad Sci USA 105:12593–8 [PubMed: 18689685]

Hilgetag CC, Grant S (2010) Cytoarchitectural differences are a key determinant of laminar projection origins in the visual cortex. Neuroimage 51:1006–17 [PubMed: 20211270]

Hilgetag CC, Medalla M, Beul SF, Barbas H (2016) The primate connectome in context: Principles of connections of the cortical visual system. Neuroimage 134:685–702 [PubMed: 27083526]

Horvát S, Gămănuţ R, Ercsey-Ravasz M, Magrou L, Gămănuţ B, Van Essen DC, Burkhalter A, Knoblauch K, Toroczkai Z, Kennedy H (2016) Spatial embedding and wiring cost constrain the functional layout of the cortical network of rodents and primates. PLoS Biol 14(7):e1002512 [PubMed: 27441598]

Hupé JM, James AC, Payne BR, Lomber SG, Girard P, Bullier J (1998) Cortical feedback improves discrimination between figure and background by V1, V2 and V3 neurons. Nature 20;394(6695):784–7

Iwamura Y, Tanaka M, Sakamoto M, Hikosaka O (1983a) Functional subdivisions representing different finger regions in area 3 of the first somatosensory cortex of the conscious monkey. Exp Brain Res 51:315–326

Iwamura Y, Tanaka M, Sakamoto M, Hikosaka O (1983b) Converging patterns of finger representation and complex response properties of neurons in area 1 of the first somatosensory cortex of the conscious monkey. Exp Brain Res 51:327–337

Iwamura Y, Tanaka M, Sakamoto M, Hikosaka O (1993) Rostrocaudal gradients in the neuronal receptive field complexity in the finger region of the alert monkey's postcentral gyrus. Exp Brain Res 92: 360–368 [PubMed: 8454001]

Iwamura Y (1998) Hierarchical somatosensory processing. Curr Opin Neurobiol 8:522–8 [PubMed: 9751655]

Jeffs J, Ichida JM, Federer F, Angelucci A (2009) Anatomical evidence for classical and extra-classical receptive field completion across the discontinuous horizontal meridian representation of primate area V2. Cereb Cortex 19:963–81 [PubMed: 18755777]

Juliano SL, Friedman DP, Eslin DE (1990) Corticocortical connections predict patches of stimulus-evoked metabolic activity in monkey somatosensory cortex. J Comp Neurol 298:23–39 [PubMed: 1698827]

Lipton ML, Liszewski MC, O'Connell MN, Mills A, Smiley JF, Branch CA, Isler JR, Schroeder CE (2010) Interactions within the hand representation in primary somatosensory cortex of primates. J Neurosci 30:15895–903 [PubMed: 21106828]

Lund JS, Angelucci A, Bressloff PC (2003) Anatomical substrates for functional columns in macaque monkey primary visual cortex. Cereb Cortex 13:15–24 [PubMed: 12466211]

Lund JS, Yoshioka T, Levitt JB (1993) Comparison of intrinsic connectivity in different areas of macaque monkey cerebral cortex. Cereb Cortex 3:148–62 [PubMed: 8490320]

Malach R, Amir Y, Harel M, Grinvald A (1993) Relationship between intrinsic connections and functional architecture revealed by optical imaging and in vivo targeted biocytin injections in primate striate cortex. Proc Natl Acad Sci U S A 90(22):10469–73. [PubMed: 8248133]

Mancini F, Haggard P, Iannetti GD, Longo MR, Sereno MI (2012) Fine-grained nociceptive maps in primary somatosensory cortex. J Neurosci 32:17155–62 [PubMed: 23197708]

Markov NT, Ercsey-Ravasz M, Van Essen DC, Knoblauch K, Toroczkai Z, Kennedy H (2013) Cortical high-density counterstream architectures. Science 342:1238406 [PubMed: 24179228]

Markov NT, Vezoli J, Chameau P, Falchier A, Quilodran R, Huissoud C, Lamy C, Misery P, Giroud P, Ullman S, Barone P, Dehay C, Knoblauch K, Kennedy H (2014) Anatomy of hierarchy: feedforward and feedback pathways in macaque visual cortex. J Comp Neurol 522:225–59 [PubMed: 23983048]

Markov NT, Misery P, Falchier A, Lamy C, Vezoli J, Quilodran R, Gariel MA, Giroud P, Ercsey-Ravasz M, Pilaz LJ, Huissoud C, Barone P, Dehay C, Toroczkai Z, Van Essen DC, Kennedy H, Knoblauch K (2011) Weight consistency specifies regularities of macaque cortical networks. Cereb Cortex 21(6):1254–72. [PubMed: 21045004]

Merzenich MM, Nelson RJ, Kaas JH, Stryker MP, Jenkins WM, Zook JM, Cynader MS, Schoppmann A. 1987 Variability in hand surface representations in areas 3b and 1 in adult owl and squirrel monkeys. J Comp Neurol 258:281–296. [PubMed: 3584541]

Negwer M, Liu YJ, Schubert D, Lyon DC (2017) V1 connections reveal a series of elongated higher visual areas in the California ground squirrel, Otospermophilus beecheyi. J Comp Neurol 525:1909–1921 [PubMed: 28078786]

Négyessy L, Pálfi E, Ashaber M, Palmer C, Jákli B, Friedman RM, Roe AW (2013) Intrinsic horizontal connections process global tactile features in the primary somatosensory cortex: Neuroanatomical evidence. J Comp Neurol 521:2798–2817 [PubMed: 23436325]

Négyessy L, Pálfi E, Ashaber M, Zalányi L, Palmer C, Kántor O, Friedman RM, Roe AW (2015) Complementary role of intra- and inter-areal cortical connections in somatosensory processing in primates Society for Neuroscience. Chicago, USA

Négyessy L, Pálfi E, Zalányi L, Ashaber M, Palmer C, Kántor O, Friedman RM, Roe AW (2016) Comparison of intrinsic and inter-areal cortical connectivity in the somatosensory cortex. IBRO Workshop Budapest, Hungary

Paul RL, Merzenich M, Goodman H (1972) Representation of slowly and rapidly adapting cutaneous mechanoreceptors of the hand in Brodmann's areas 3 and 1 of Macaca mulatta. Brain Res 36:229–49 [PubMed: 4621596]

Pálfi E, Zalányi L, Ashaber M, Palmer C, Friedman RM, Roe AW, Négyessy L (2016) Intrinsic and interareal connections in the primate somatosensory cortex. 10th FENS Forum of Neuroscience Copenhagen, Denmark

Pearson RC, Powell TP (1978) The cortico-cortical connections to area 5 of the parietal lobe from the primary somatic sensory cortex of the monkey. Proc R Soc Lond B Biol Sci 200:103–8 [PubMed: 24219]

Pei YC, Denchev PV, Hsiao SS, Craig JC, Bensmaia SJ (2009) Convergence of submodality-specific input onto neurons in primary somatosensory cortex. J Neurophysiol 102:1843–53 [PubMed: 19535484]

Rasch MJ, Chen M, Wu S, Lu HD, Roe AW (2013) Quantitative inference of population response properties across eccentricity from motion-induced maps in macaque V1. J Neurophysiol 109:1233–49 [PubMed: 23197457]

Reed JL, Pouget P, Qi HX, Zhou Z, Bernard MR, Burish MJ, Haitas J, Bonds AB, Kaas JH (2008) Widespread spatial integration in primary somatosensory cortex. Proc Natl Acad Sci USA 105:10233–10237 [PubMed: 18632579]

Reed JL, Qi HX, Pouget P, Burish MJ, Bond AB, Kaas JH (2010a) Modular processing in the hand representation of primate primary somatosensory cortex coexists with widespread activation. J Neurophysiol 104:3136–3145 [PubMed: 20926605]

Reed JL, Qi HX, Zhou Z, Bernard MR, Burish MJ, Bonds AB, Kaas JH (2010b) Response properties of neurons in primary somatosensory cortex of owl monkeys reflect widespread spatiotemporal integration. J Neurophysiol 103:2139–2157

Rockland KS (2015) About connections. Front Neuroanat 9:61 [PubMed: 26042001]

Roe AW, Ts'o DY (2015) Specificity of V1-V2 Orientation Networks in the Primate Visual Cortex. Cortex 72: 168–78. [PubMed: 26314798]

Sathian K (2016) Analysis of haptic information in the cerebral cortex. J Neurophysiol 116(4):1795–1806 [PubMed: 27440247]

Sincich LC, Blasdel GG (2001) Oriented axon projections in primary visual cortex of the monkey. J Neurosci 21:4416–4426 [PubMed: 11404428]

Sincich LC, Jocson CM, Horton JC (2010) V1 interpatch projections to v2 thick stripes and pale stripes. J Neurosci 30:6963–6974 [PubMed: 20484638]

Sporns O (2015) Cerebral cartography and connectomics. Philos Trans R Soc B Biol Sci 370(1668): 1–12

Sripati AP, Yoshioka T, Denchev P, Hsiao SS, Johnson KO (2006) Spatiotemporal receptive fields of peripheral afferents and cortical area 3b and 1 neurons in the primate somatosensory system. J Neurosci 26:2101–2114 [PubMed: 16481443]

Stettler DD, Das A, Bennett J, Gilbert CD (2002) Lateral connectivity and contextual interactions in macaque primary visual cortex. Neuron 36:739–50 [PubMed: 12441061]

Sur M, Garraghty PE, Bruce CJ (1985) Somatosensory cortex in macaque monkeys: laminar differences in receptive field size in areas 3b and 1. Brain Res 342:391–5 [PubMed: 4041845]

Sur M, Merzenich MM, Kaas JH (1980) Magnification, receptive-field area, and "hypercolumn" size in areas 3b and 1 of somatosensory cortex in owl monkeys. J Neurophysiol 44: 295–311 [PubMed: 7411189]

Sur M, Nelson RJ, Kaas JH (1982) Representations of the body surface in cortical areas 3b and 1 of squirrel monkeys: comparisons with other primates. J Comp Neurol 211:177–92 [PubMed: 7174889]

Sur M, Wall JT, Kaas JH (1981) Modular segregation of functional cell classes within the postcentral somatosensory cortex of monkeys. Science 212:1059–1061 [PubMed: 7233199]

Thakur PH, Fitzgerald PJ, Hsiao SS (2012) Second-order receptive fields reveal multidigit interactions in area 3b of the macaque monkey. J Neurophysiol 108:243–62 [PubMed: 22457468]

Ts'o DY, Gilbert CD (1988) The organization of chromatic and spatial interactions in the primate striate cortex. J Neurosci 8(5): 1712–1727. [PubMed: 3367218]

Vezoli J, Falchier A, Jouve B, Knoblauch K, Young M, Kennedy H (2004) Quantitative analysis of connectivity in the visual cortex: extracting function from structure. Neuroscientist 10:476–82 [PubMed: 15359013]

Vincis R, Fontanini A (2016) A gustocentric perspective to understanding primary sensory cortices. Curr Opin Neurobiol 40:118–124 [PubMed: 27455038]

Wandell BA, Winawer J (2015) Computational neuroimaging and population receptive fields. Trends Cogn Sci 19:349–57 [PubMed: 25850730]

Wang Z, Chen LM, Négyessy L, Friedman RM, Mishra A, Gore JC, Roe AW (2013) The relationship of anatomical and functional connectivity to resting-state connectivity in primate somatosensory cortex. Neuron 78:1116–26 [PubMed: 23791200]

Yarch J, Federer F, Angelucci A (2017) Local circuits of V1 layer 4B neurons projecting to V2 thick stripes define distinct cell classes and avoid cytochrome oxidase blobs. J Neurosci 37:422–36 [PubMed: 28077720]

Yau JM, Kim SS, Thakur PH, Bensmaia SJ (2016) Feeling form: the neural basis of haptic shape perception. J Neurophysiol 115:631–42 [PubMed: 26581869]

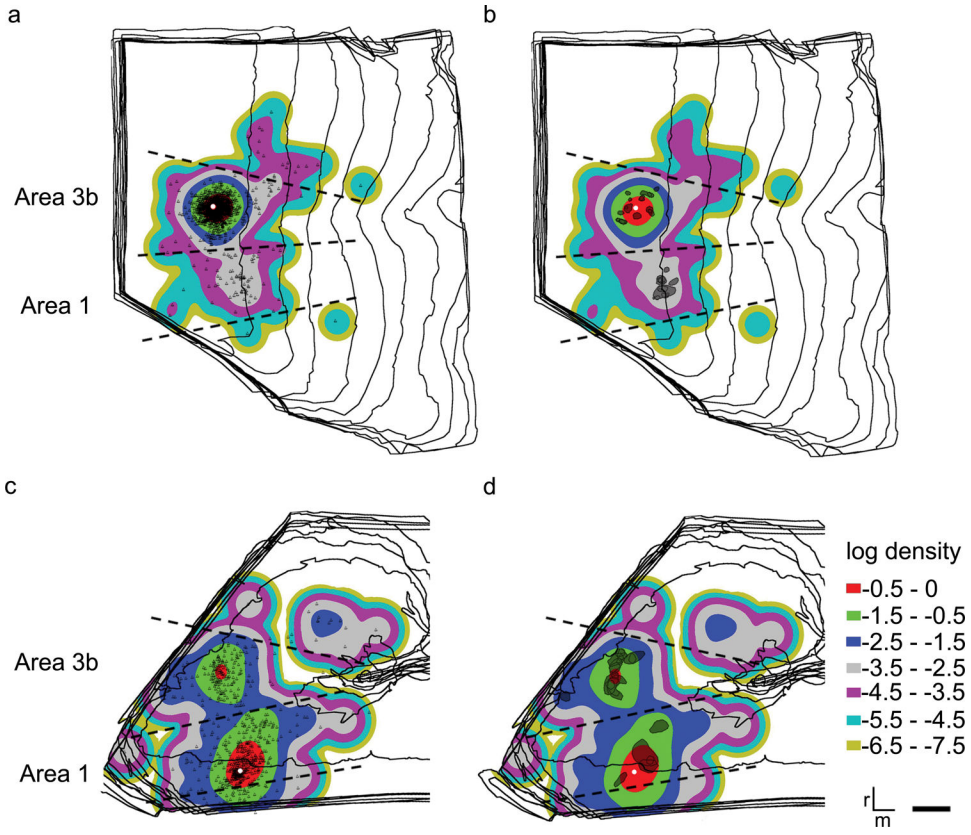

Figure 1. Distribution of the retrograde and anterograde labeling.

Kernel density maps of retrograde labeling superimposed (a, c) by the actual distribution of BDA-labeled neurons (small black triangles) and (b, d) by the distribution of anterogradely labeled terminal axon arborizations or axonal patches (gray shading) are shown in examples following area 3b (a, b) and area 1 (c, d) injections. The density of neuronal labeling (log scale) is indicated by different colors. Note on A, the high density of labeled neurons near the injection site completely overlap and occlude the red colored area of the kernel density map. Note also the spatially restricted localization of the high density connections and a more diffuse distribution of low density connections. Black lines show the outline of the sections, dashed lines show the area borders, white dot indicates the injection site. Scale bar: 1 mm. r: rostral, m: medial.

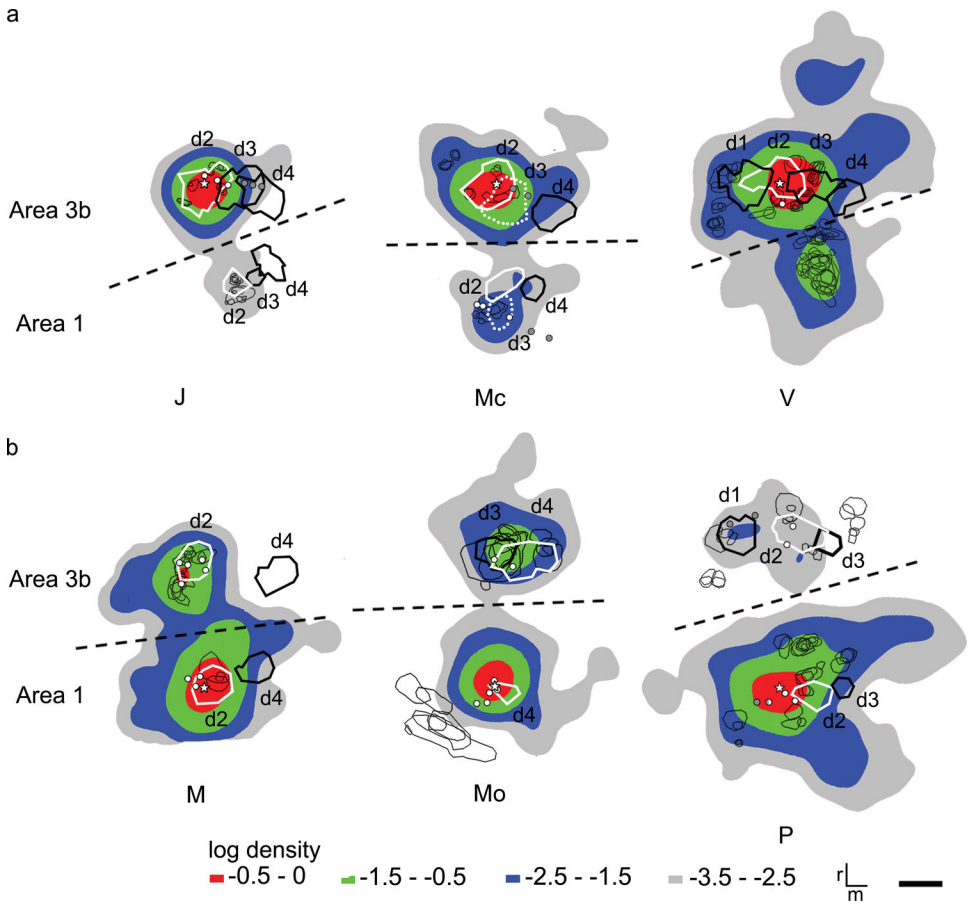

Figure 2. Distribution of the highest density of projection neurons and efferent axonal patches.

(a, b) Kernel density maps show the spatial distribution of BDA-labeled projection neurons after area 3b (a) and area 1 (b) injections for the six cases. The four highest densities of neuronal labeling are indicated by different colors. Overlain is the distribution of the groups of overlapping anterogradely labeled axonal patches forming groups, marked by thin contours, after merging across the serial sections. The location of the OIS activation-area of the injected distal finger pad representations (d2 in 5 cases, d4 in Mo) are shown by thick white contours, the OIS activation of the neighboring finger pads are shown with thick black contours. In case Mc the OIS activation-area of the neighboring finger pad (d3) is also highlighted by white dotted contour; because of the large overlap between these two representations in area 3b made specifying the exact somatotopic representation of the injection uncertain. The results of electrophysiological mapping of the injected (white dots) and one of the neighboring (grey dots marking d3 tip in J and MC and d1 tip in P; note half grey-half white dot showing mixed d1/d2 response properties in area 1 of cases P) distal finger pad representations are also superimposed. Note that the injection sites (white star) were also verified by electrophysiological mapping and also represent a recording site. Note the high overlap between the OIS-area and the highest density neuronal labeling as well as the crowding of the axonal patches, especially in case of the inter-areal labeling. Note also the lack of OIS activation in area 1 of case V. All the other conventions are the same as in Figure 1. Scale bar: 1 mm.

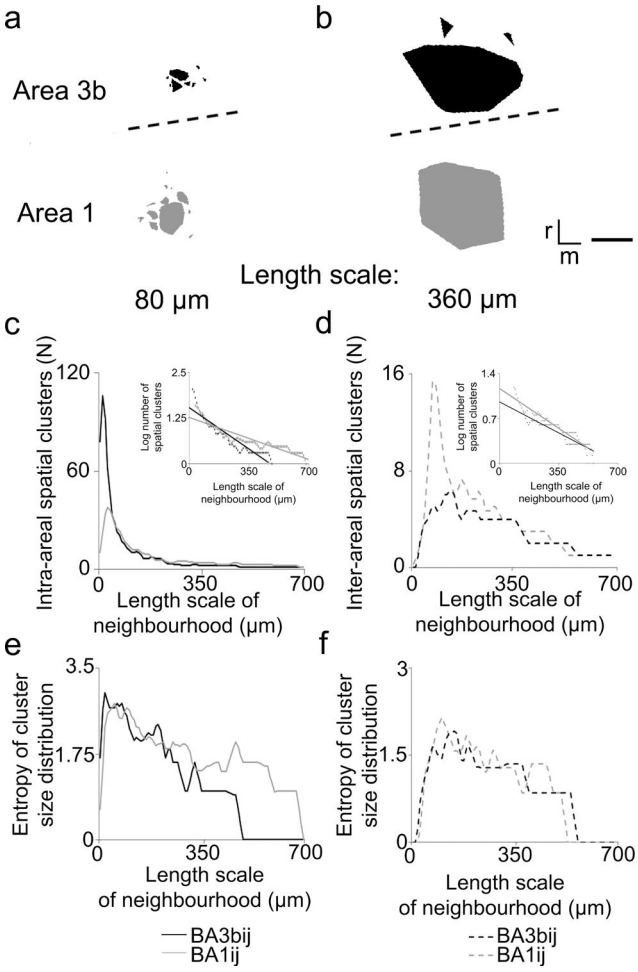

Figure 3. The results of density based clustering (DBSCAN) of the retrogradely labeled neurons at different length scales.

(a, b) Panels show the number, size and distribution of clusters for both the intra-areal and inter-areal labeling at two length scales in a case with area 1 injection (BA1ij). Black labels clusters in area 3b (BA3b) and grey labels clusters in area 1. The highest density labeling results in the emergence of a large central cluster flanking by smaller ones especially within the injected area. Borders between areas are marked by dashed lines. r: rostral, m: medial. Scale bars represent 1 mm. (c, d) Number of clusters of retrogradely labeled neurons based on density-based spatial clustering (DBSCAN) is presented as the function of the length scale (see Methods) for the intra-areal (c) and the inter-areal (d) labeling. The number of clusters quickly reached a peak as the function of the length scale and then decayed at a slower rate until reaching a minimum number. Insets show the slopes of the fitted lines on log-linear plots of the cluster number (panel c, area 3b injection (BA3bij): −0.0032, area 1 injection: −0.0016) (panel d, area 3b injection: −0.0014, area 1 injection: −0.0018). Data on insets are plotted only from the peak values. Note the location of the peak at different length scales in the different cases (black vs. grey dots in c and d). (e, f) Entropy measure of the variability of the cluster size distribution is shown. Plots show the median of the six cases. For better visibility the curves were smoothed by moving average with a 3 datapoint (24 μm)

window size. Note that at larger length scales the entropy remained relatively high compared to the large drop of the number of clusters.

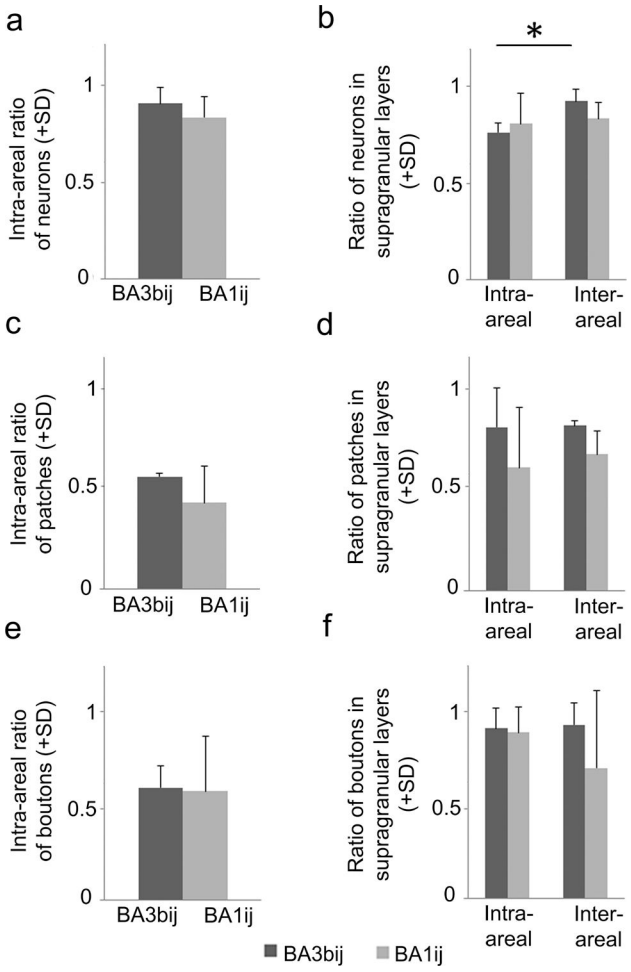

Figure 4. Areal and laminar distribution of the BDA labeled neuronal elements.

Proportion of intra-areal vs. inter-areal labeled neurons (a), terminal axon arborizations (c) and bouton-like structures in terminal axon arborizations (e). Fraction of supragranular vs. infragranular labeled neurons (b), terminal axon arborizations (d) and bouton-like structures in terminal axon arborizations (f). Calculations of proportional distributions were made as follows. The fraction of labeled structures in area 3b (BA3b) and area 1 (BA1) was determined by considering the total counts within the two areas. The laminar distribution was calculated as the proportion of labeled structures in the supragranular sections relative to the total number of labeled structures across all the sections within an area studied. Asterisk (*) indicate statistically significant difference.

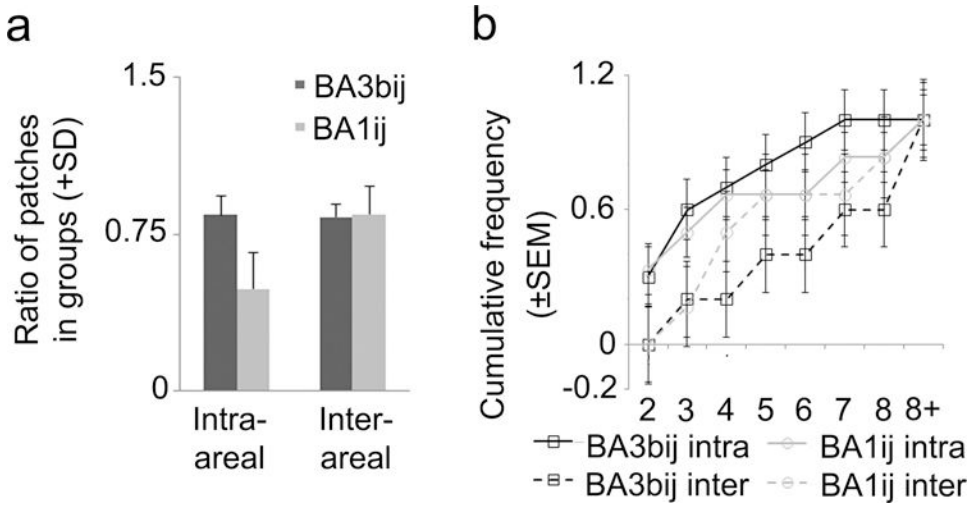

Figure 5. Size distribution of axonal patch groups.

(a) Intra-areal and inter-areal ratio of the axonal patches found in groups following injections into area 3b or 1 (BA3b and BA1, respectively). (b) Cumulative frequency histograms of the size of the patch groups for the 4 different categories of labeling. In the different cases the number of sections varied from 8–16 except one case with only 5 sections.

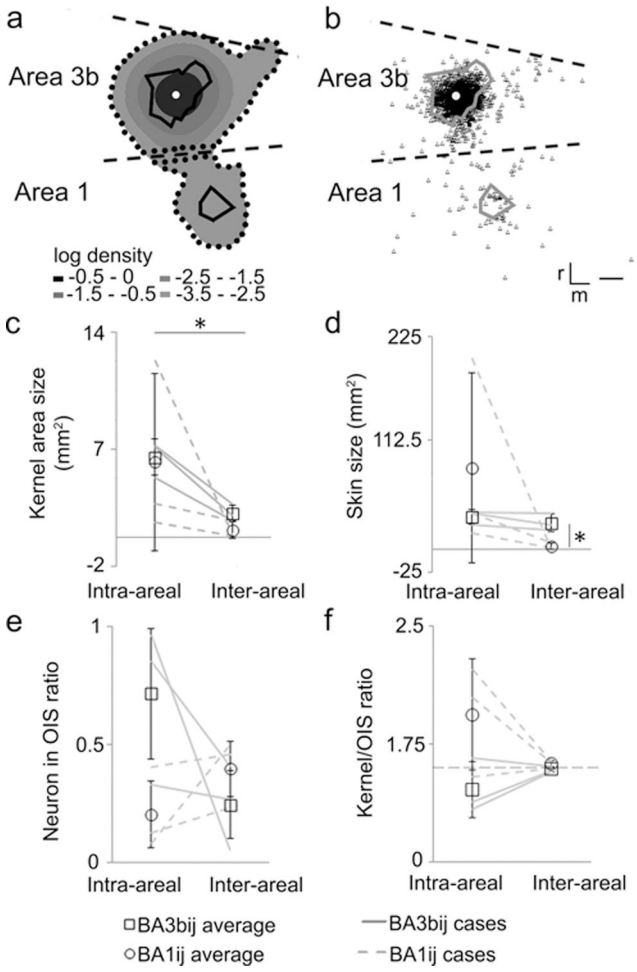

Figure 6. Spatial spread of the projection neurons.

(a) Kernel density map superimposed with the OIS activation (black thick contours) of the injected distal finger pad representations in case of J after area 3b injection (BA3bij). Dotted contours enclose the equal density areas used for comparisons. (b) Distribution of the BDA-labeled neurons (small black triangles) superimposed with the OIS activation of the injected distal finger pad representations (thick grey contours) in the same case as in a. In a and b all the other conventions are the same as in Figure 1. Scale bar represents 1 mm. (c) Size of intra- and inter-areal labeling of equivalent thresholds (as shown by the dotted contours in a) of neuronal kernel density after area 3b injection and area 1 injection (BA1ij). (d) Size of the patch of skin represented by the kernel regions after adjusting for the cortical magnification factors of areas 3b and 1. (e) Ratio of labeled neurons within an activated region determined by OIS (as shown in panel b). (f) Size of the highest neuronal density kernel area relative to the OIS-area. For f, kernel densities were computed separately for the intra-areal and inter-areal labeling (Table 1). (e, f) For area 1 of case V the average OIS-area reported in Friedman et al. (2008) was used for the calculations. Error bars on averages represent ±SD. Asterisk (*) indicate statistically significant difference.

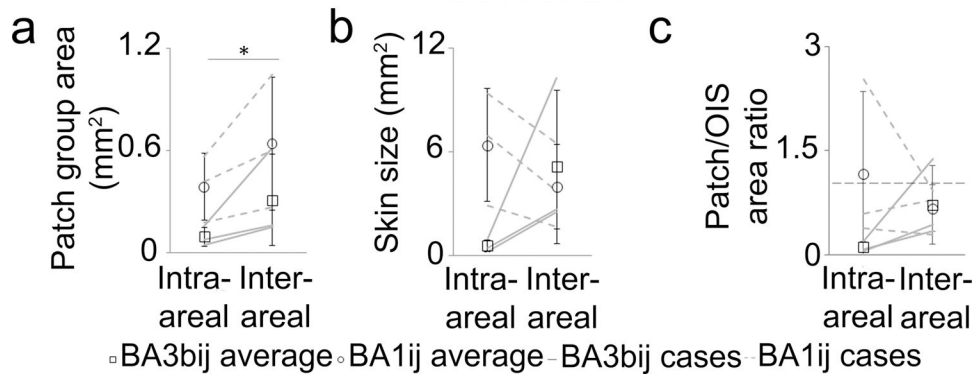

Figure 7. Size of the efferent axonal patch groups and the represented skin areas.

(a) Size of the patch groups. (b) Size of the skin area represented by the patch groups after consideration of the CMFs. (c) Ratio relating the average areas of the patch groups with respect to OIS-areas. Except for the intra-areal value of with area 3b injection (BA3bij), the ratios approach 1, suggesting comparable sizes for the patch groups and OIS-areas. BA1ij: area 1 injection.

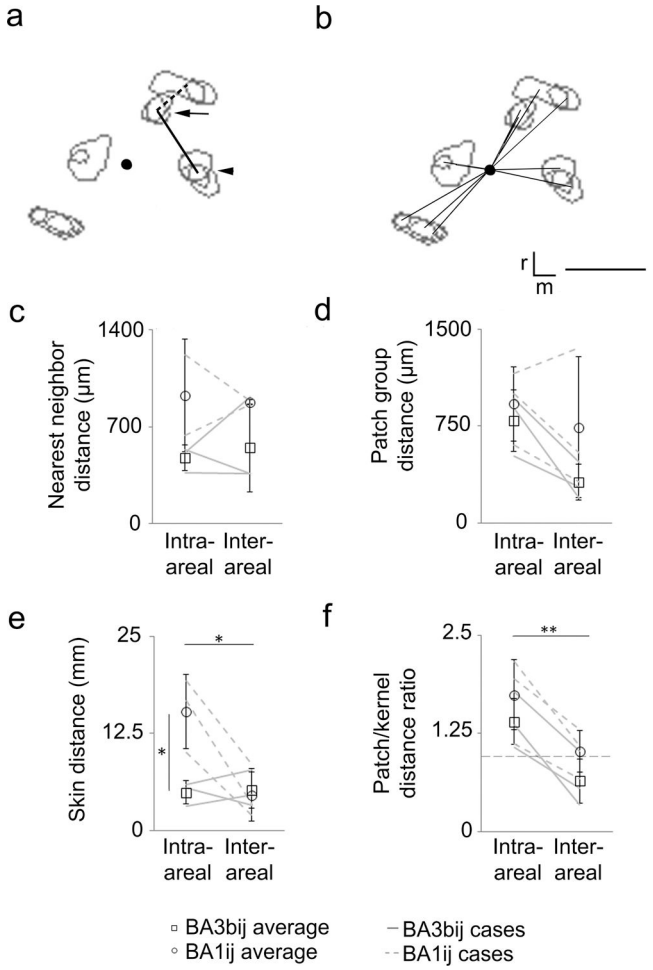

Figure 8. Spatial spread of efferent axonal patches

(a) Example shows the nearest neighbor measurement (shown in c) of the patch groups (grey contours) in case J with an injected area 3b. The nearest neighbor of the patch group indicated by the arrowhead is connected by the straight line while that of the patch group shown by the arrow is connected by the dashed line. (b) An example for the patch group distance measurement (d) in the injected area in case J after area 3b injection. Black lines show the distance between the center of mass of the patches and the injection site. In a and b black dot indicates the injection site. r: rostral, m: medial. Scale bar represents 1 mm. (c) Average distance between the nearest patch groups (as shown on a). There is a greater tendency towards a looser packing density (larger distances) after area 1 injection. However, only two cases of area 1 injections could be presented as case M only exhibited single intra-areal and inter-areal patch groups. (d) Average distances are shown from the injection site in case of the intra-areal labeling or from the center of mass of the highest density retrograde labeling on the kernel maps in case of the inter-areal labeling (as shown on B). (e) Size of the patch of skin represented by the average cortical distance of the patch groups (d) after adjusting for the cortical magnification factors of areas 3b and 1. (f) Ratio comparing the average distance of patch groups from the center (d) relative to the radius of the highest kernel density area (see description in the text). The highest kernel density areas were

independently computed for the inter- and intra-areal labeling (Table 1). Error bars represent the ±SD. Asterisk (*) indicate statistically significant difference.

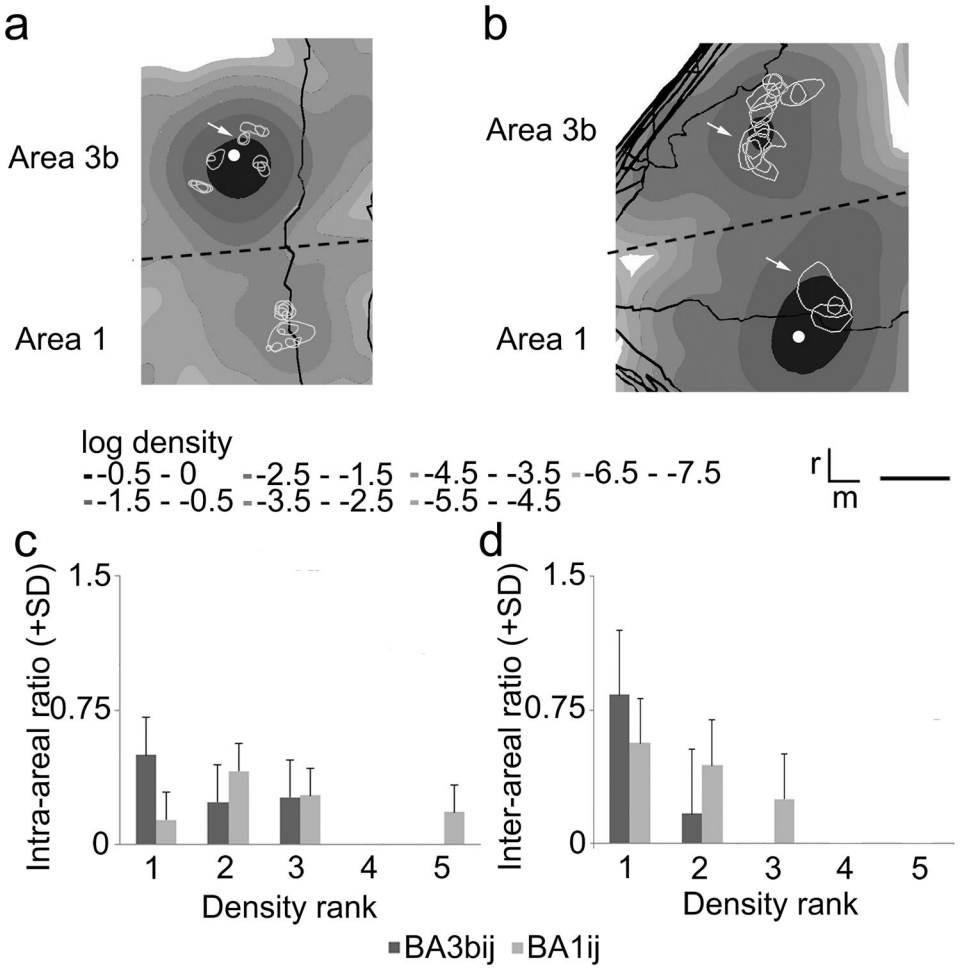

Figure 9. Distribution of efferent axonal patches relative to the density of the projection neurons.

(a, b) Kernel density maps (grey shading) superimposed by the efferent axonal patch groups (white contours) after area 3b (a) and area 1 (b) injection (BA3bij and BA1ij, respectively). Note that the full range of densities are shown. White arrows show patch groups overlapping the two highest densities ranked 1 and 2 in these cases. In case a patch group overlapped with two densities 0.5 was counted for each overlapping densities. Conventions are the same as in Figure 1. Scale bar on b represents 1000 μm on a, b. (c, d) Relationship of the patch group distribution and neural kernel density following injections of area 3b and area 1. For a better comparability between cases the log densities were ranked beginning with the highest density where a patch group could be detected in each case. Intra-areal (c) and inter-areal (d) distributions appear similar. After area 3b injection patches are concentrated in areas of higher retrograde labeling densities, while after area 1 injection patches are more widely distributed.

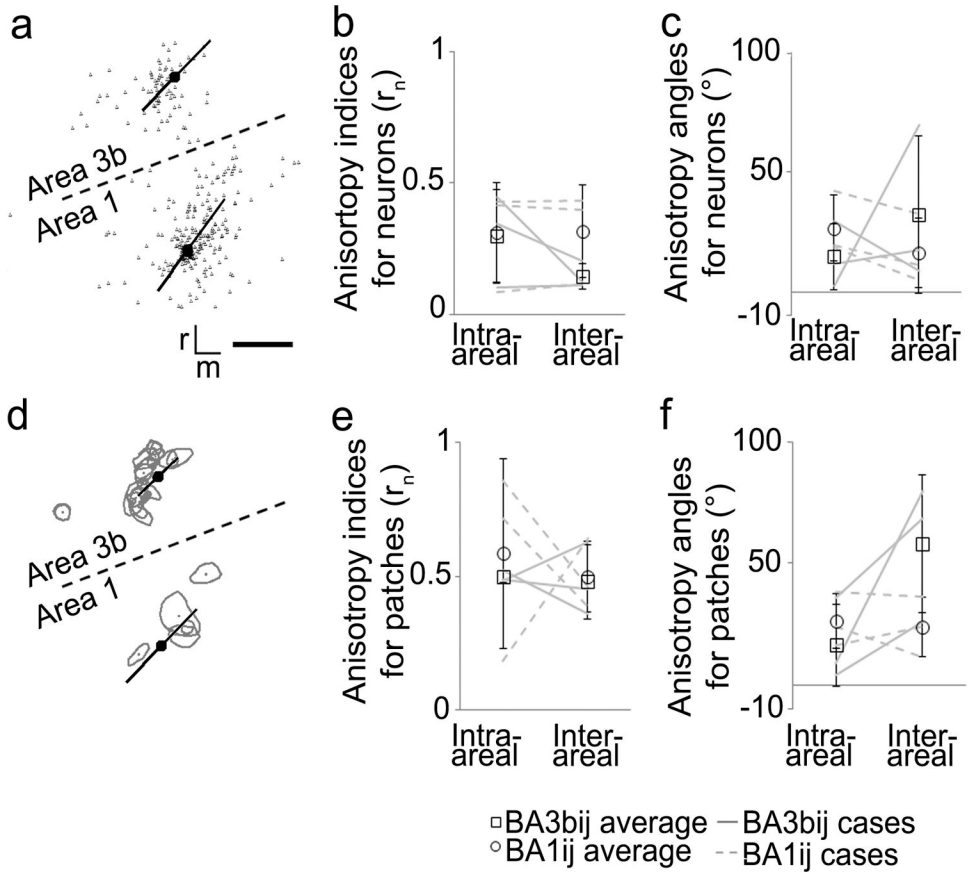

Figure 10. Anisotropy of the distribution of projection neurons and efferent axonal patches.

(a, d) Examples showing the neurons (a) and axonal patches (d) and computed anisotropy vectors (r_n, black lines bisected by a dot) for case M after the injection of area 1. Axonal patches are represented by grayish contours with dots in the middle representing the center of mass (d). (b, c, e, f) Plots show intra-areal and inter-areal anisotropy (r_n, b, e) and anisotropy angle (c, f) averaged across cases for the labeled neurons (b, c) and patches (e, f). An anisotropy angle of 0 or 90 degrees would indicate an orientation across or parallel to the representation of the finger pads, respectively. Note that on e and f anisotropy and angle was computed by considering all the efferent patches including the single ones. BA3bij: area 3b injection, BA1ij: area 1 injection. Dashed lines on a, d show area borders. r: rostral, m: medial. Scale bars represent 1 mm. Error bars represent the SD.

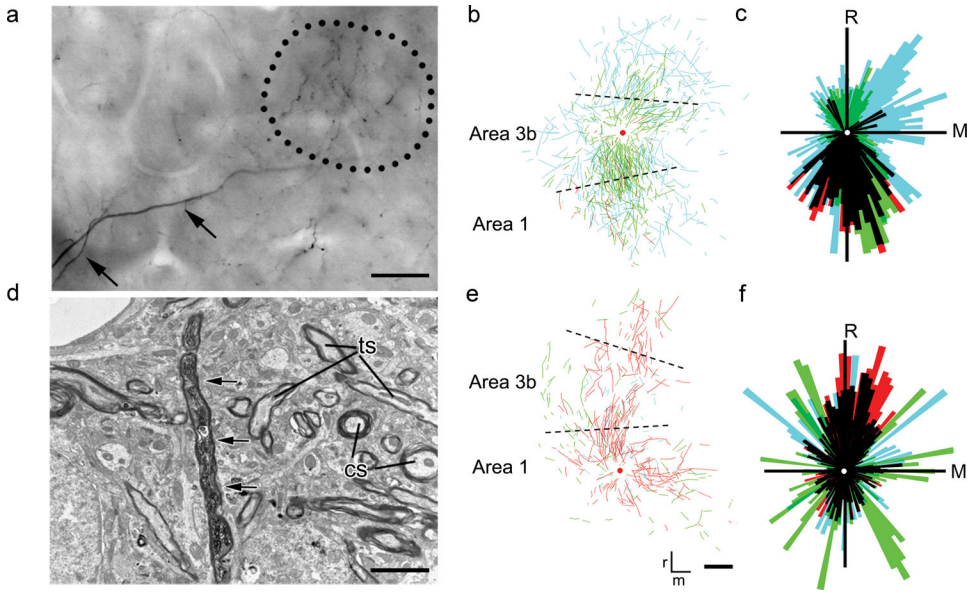

Figure 11. Distribution of BDA-labeled thick and smooth axonal processes.

(a, d) Light (a, *black arrows*) and electron (d, black arrows) microscopic image showing a thick and smooth fiber and a myelinated fiber, respectively. *Dotted circle* on (a) outlines an axonal patch. Note several BDA-negative cross- and tangential sections (cs and ts, respectively) of myelinated axons in the vicinity of the labeled one. (b, e) Reconstructions of the thick and smooth axonal processes of the different cases are overlaid separately for area 3b injections (b) and area 1 injections (e). *Dashed lines* show the area borders; red dot indicates the injection site. (c, f) Polar plots showing the preferred direction of the orientation of labeled axons after aligning the different cases following area 3b (c) and area 1 (f) injections. The *different colors* indicate the labeled axons of the individual cases. *Black* lines indicate the orientations with highly overlapping distributions for the two groups of injections. Intersection of the axes on (c, f) represents the injection sites where the white dot indicates the injection sites. Scale bar on (a) is 25 μm, on (d) is 2 μm, on (b, e) is 1 mm. r,R: rostral, m,M: medial.

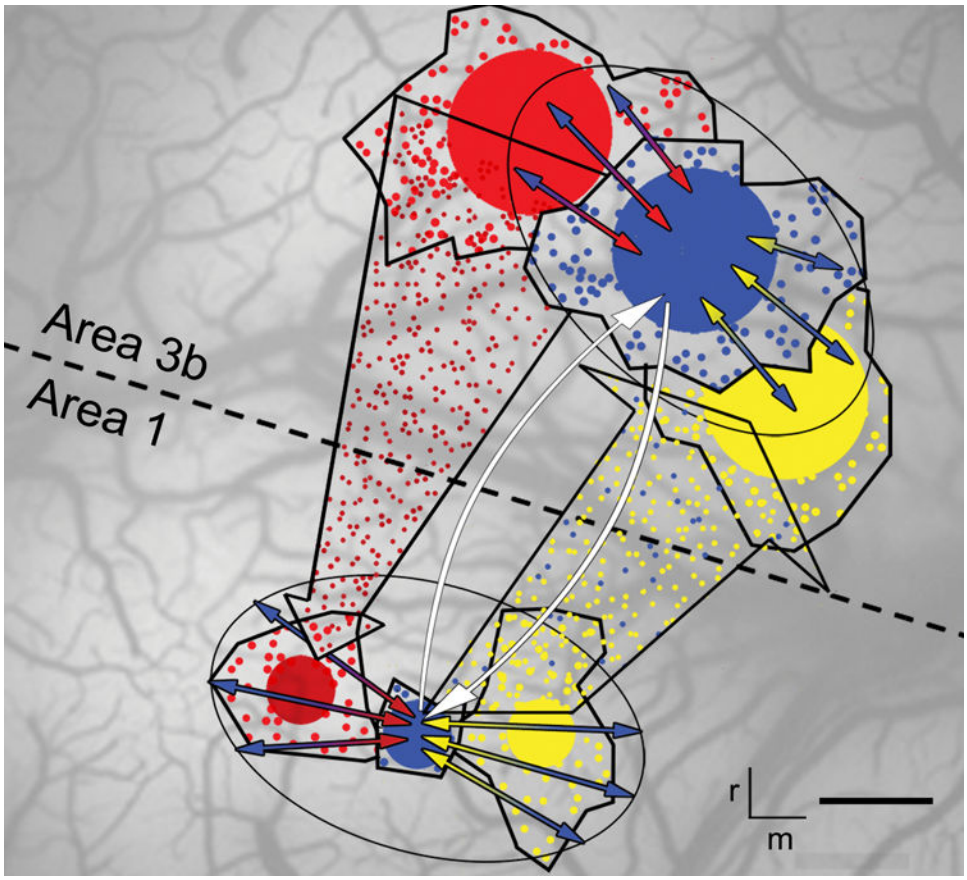

Figure 12. The connectional motif of the columnar circuitry within and between two neighboring areas in SI.

The schematic summarizes the quantitative evidence that support the organization of the intra-areal and inter-areal connectivity of a column size cortical domain of area 3b and area 1. Intrinsic connections exhibit a similar, large spread across the finger representations in the two areas (full, colored arrows within ellipsoids) (Fig. 6c). However, considering both the origin and termination feedforward connections (large arrow with red dots) is largely convergent and more tightly packed compared to the more divergent and loosely packed distribution of the feedback (large arrow with yellow and blue dots) connections (Fig. 8c, d, 9). The patterning of dot symbols represents the density and clustering of the projection neurons, which are higher in area 3b than in area 1 (Fig. 3c, d). Also, due to the different CMFs (shown by the different size of the outlined regions (OIS-area) which also include the filled circles with different sizes symbolizing the different proportion of projection neurons localized within the OIS-area), the lateral spread of connections converge on a larger skin surface in area 1 than in area 3b (Figs. 6d, 8e). White arrows show a reciprocal pathway formed by feedforward and feedback connections, which is responsible for fast information exchange between homotopic finger representations (Fig. 11). Note also the anisotropic, mediolateral distribution of the connections including both the projection neurons and efferent axonal patches (Fig. 10). The different colors represent connections of different

distal finger pad representations. Schematic is superimposed on the cortical surface of an experimental case. Scale bar represents 500 μm. Orientation bars: r: rostral and m: medial.

Table 1.

Size (x10^5 μm^2±SD) of the highest density areas identified after computing the kernel density maps separately for the intra-areal and inter-areal retrograde labeling.

Injected area	**area3binj**		**area1inj**	
Area of measurement	**area 1**	**area 3b**	**area 1**	**area 3b**
Highest density region	6.2±0.9	7.5±1.2	6.4±1.8	10.6±9.4
Skin area	103.3 ±14.7*	47.1 ±7.7	106.0 ±30.1	66.1±58.4

Asterisk indicates a significantly larger intra-areal than inter-areal value. Numbers indicate averages±SD. Note the large value for feedforward projection neurons (area 3b data after area 1 injection) in row one, which is in contrast to what is shown in Figure 5a. This is in correspondence with the larger inter-areal labeling density following area 1 injection (Fig. 2) and the high fraction of neurons within the OIS-area (Fig. 6c).